THE TERRESTRIAL LASER SCANNER FOR CASSAVA (*Manihot esculenta*) PHENOTYPING & THE DEVELOPMENT OF A LOW-COST 3D PHENOTYPING PLATFORM

A Dissertation

by

RICHARD KYLE BRUTON

Submitted to the Office of Graduate and Professional Studies of
Texas A&M University
in partial fulfillment of the requirements for the degree of

DOCTOR OF PHILOSOPHY

Chair of Committee,	Dirk B. Hays
Committee Members,	Marian Eriksson
	Russell W. Jessup
	Nithya Rajan
Head of Department,	David D. Baltensperger

May 2020

Major Subject: Plant Breeding

ABSTRACT

There will be a large increase in the world's population over the coming decades, which will require a significant increase in global food production. However, a large gap exists between the cultivars we plant today and those required to feed the world of tomorrow. We currently lack the ability to rapidly phenotype for those improved cultivars, causing a bottleneck in the breeding process. One tool which might speed up the phenotyping process is LIDAR, or light detection and ranging. This technology has proven useful in the phenotyping of many characteristics across a number of crops; however, it has not been demonstrated on cassava. Cassava is of global importance as both a source of starch as well as a foodstuff for cattle and, to a lesser extent, as a leafy vegetable. We demonstrate the applicability of using terrestrial LIDAR for the determination of cassava height, as well as total aboveground biomass and total leaf biomass, all within a field setting. In addition, we showcase the development of a novel, low-cost 3D phenotyping platform designed around Microsoft Kinect V2 sensors. The platform was designed to combat the high acquisition costs generally associated with, and limiting of, the study of 3D high-throughput phenotyping.

DEDICATION

I would like to dedicate this writing to my parents, Nuell and Marion. This work is a testament to their unwavering support bestowed upon me during this academic pursuit.

I would also like to dedicate this to my best friend and future wife, Shruti Surya.

Meow…

ACKNOWLEDGEMENTS

I would like to thank my committee chair, Dr. Hays, and my committee members, Dr. Eriksson, Dr. Jessup, and Dr. Rajan, for their guidance and support throughout the course of this research. In addition, I would like to thank Dr. Bruce Gooch for his many hours of time spent brainstorming my work.

I would like to think my lab mates, both at Texas A&M and at the Center for Tropical Agriculture in Cali, Colombia. If not for them, this work would never have come to fruition.

Thanks also to my friends, colleagues and the departmental faculty and staff for their many hours of teaching, listening and guiding.

CONTRIBUTORS AND FUNDING SOURCES

Contributors

This work was supervised by a dissertation committee consisting of the chair Dr. Dirk B. Hays and committee members Dr. Russell Jessup and Dr. Nithya Rajan of the Department of Soil and Crop Science, as well as Dr. Marian Eriksson of the Department of Ecosystem Science and Management.

The data presented in Chapters 3 and 4 was made possible in part by Dr. Michael Selvaraj of the International Center for Tropical Agriculture in Cali, Colombia. The work depicted in Chapter 5 was completed in part by Tyler Adams and Henry Ruiz of the Molecular and Environmental Plant Sciences Department.

All other work conducted for the dissertation was completed by the student independently.

Funding Sources

This work was made possible by The National Science Foundation under Grant Number 1543957. Its contents are solely the responsibility of the authors and do not necessarily represent the official views of the Plant Genome Research Resource or the BM Gates Foundation.

Additional funding was provided by The Borlaug Foundation under the U.S. Borlaug Fellows in Global Food Security Program.

NOMENCLATURE

ALS	aerial laser scanning
CC	CloudCompare
CIAT	International Center for Tropical Agriculture
CT	X-ray computed tomography
EB	early bulking
G X E	gene by environment
GUI	graphical user interface
IR	infrared
IITA	International Institute of Tropical Agriculture
LAD	leaf area density
LAI	leaf area index
LICF	laser-induced chlorophyll florescence
LIDAR	light detection and ranging
MRI	magnetic resonance imaging
PAD	plant area density
PMF	Progressive Morphological Filter
SBC	single board computer
SDK	software development kit
SOR	Statistical Outlier Filter
TLS	terrestrial laser scanner
TxDOT	Texas Department of Transportation

UAV	unmanned aerial vehicles
WCF	Windows Communication Foundation

TABLE OF CONTENTS

Page

Page

LIST OF FIGURES

Page

Page

LIST OF TABLES

Page

CHAPTER II

INTRODUCTION

By 2050 the world's population is expected to increase by more than two billion people, driving a significant rise in global food demand (Graham-Rowe 2011). The majority of this growth is forecasted to occur in developing countries (Nations 2015) where the demand for energy is also expected to increase significantly over the coming decades (Wolfram et al., 2012). Biofuels are expected to play a major role in filling this energy gap, but they currently rely heavily on edible portions of staple crops and will undoubtedly compete with food production for arable land (Cheng & Timilsina 2011). With the increasing demand for food and bioenergy and finite resources available to meet those demands, there is a great need to increase the efficiency of crop production, especially in the developing world.

As the food shortage deepens, so will the need to maximize yield while simultaneously increasing efficiency. Data suggests the yield increases currently being achieved will not keep pace with the projected food demands within the near future (Tester & Langridge 2012). Furthermore, these yield increases are derived in part from the use of artificial inputs, mainly nitrogen fertilizer and irrigation, whose use needs to be reduced in order to combat global climate change. In the coming decades demand for resources will rise along with the expanding population, driving up their price. As a result, we should expect rising food costs and further economic uncertainty (Godfray et al., 2010).

There is a need to increase yield while reducing inputs; however, a large gap exists between the tools of today and the tools required to develop the elite cultivars of tomorrow (Araus & Cairns 2014). Specifically, a bottleneck exists within the field-based screening process,

which severely slows the development of these needed cultivars (Furbank et al., 2009; Furbank & Tester 2011). One way to remove this bottleneck is through the use of high-throughput phenotyping; a future consisting of high-throughput and early detection of desired phenotypic traits will exist only if the technological investments are made. The research proposed here will set the foundation for a generation-long pursuit towards the development of high-throughput phenotyping platforms in the struggle for worldwide food security.

Objectives

1) Predicting Cassava Height Using a Terrestrial Laser Scanner Under Field Conditions:

   Height is an important trait in many crops and is often one of the first traits to be explored in a high-throughput phenotyping context. In cassava, height is often used as a predictor of pest susceptibility and environmental stress. The terrestrial laser scanner has been used in other crops to predict height with great success, but has seen no use in the phenotyping of cassava. As a first step in this direction we used a Trimble TX5 terrestrial laser scanner in an attempt to predict height in three different cassava genotypes under field conditions.

2) Prediction of Aboveground Biomass of Three Cassava Genotypes Using a Terrestrial Laser Scanner:

   There is considerable need to develop a rapid and non-destructive method to predict cassava plant biomass under field conditions. Terrestrial laser scanners have shown to correlate well to biomass in some crop species, though the technology has not been tested in cassava. Terrestrial laser scanner data was collected under field conditions on three structurally contrasting genotypes of cassava. We hypothesized that the data captured with the terrestrial laser scanner would correlate well to the total aboveground biomass, as well as the total leaf biomass in cassava.

3) A Low Cost 3D Phenotyping Platform Using Microsoft Kinect V2 Sensors:

There is a need for 3D high-throughput phenotyping tools within the field of agriculture. While commercially available airborne and terrestrial laser scanners have proven viable for phenotyping across many crops, their high purchase cost is a major barrier to their wider application. We attempted to eliminate this cost barrier through the utilization of consumer-grade Microsoft Kinect depth cameras as a 3D phenotyping sensor. We developed a field-worthy phenotyping platform with off-the-shelf hardware, run by custom-made software, and demonstrate its applicability through a preliminary field campaign.

CHAPTER III

BACKGROUND

Cassava

Cassava (*Manihot esculenta*) is the sixth major staple crop in the world (Mann 1997). It is grown across the tropical and subtropical regions, where it provides food for over half a billion people worldwide (Prochnik et al., 2012). Within sub-Saharan Africa in 2008, 117 million tons of cassava was produced, placing it above maize in total production (Sayre et al., 2011). Within Latin America and the Caribbean, cassava plays a dual role in food security and as a feedstock, while in Asia it has become an important industrial crop.

Every part of the cassava plant has value, though the starch-rich roots are the most important economic component. The species is included in the top four starch sources worldwide along with maize (*Zea mays*), potato (*Solanum tuberosum*), and wheat (*Triticum aestivum*) (Ellis et al., 1998; Davis et al., 2003). Low levels of fat and protein in the root make the starch of excellent quality and eases extraction (Ceballos et al., 2010). Both the root and the leaf can be used as a feedstock, though the nutritional value is roughly 70% of maize, which is reflected in its lower cost. The low input requirements of cassava, along with its ability to grow under drought and nutrient-limited conditions, make the crop an attractive candidate for biofuel production (Jansson 2010). This has led China to list cassava as one of the key crops to meet their 2020 bioenergy goals (Chang et al., 2012). While these uses play an important role, the vast majority of cassava is utilized for food security by smallholder farmers where the root, and less so the foliage, is consumed (Ceballos et al., 2004).

Considering the worldwide importance of cassava, especially within developing countries, it is assumed that yield improvements would strengthen economic growth within these areas through the transition of cassava from a subsistence to a cash crop (Nassar & Ortiz 2007). Late bulking has been described as the single cause for rejection of genotypes in sub-Saharan Africa (Nweke et al., 2002). This has led many to attempt to improve yield and promote early bulking (EB) within the roots (Okogbenin & Fregene 2002; Ceballos et al., 2004). There currently is a transition to EB genotypes within sub-Saharan Africa where, in countries such as Nigeria and Ghana, the introduction of these genotypes have led to 40% higher yields without fertilizer (Nweke et al., 2002). A relationship was found between earliness in root yield and EB (Wholey & Cock 1974) with root yield being directly related to the duration and intensity of bulking (Lian & Cock 1979). It has been suggested breeding for EB genotypes would have two significant advantages; a shortening of crop duration and increased yield (Okogbenin & Fregene 2002). The main roadblock to the development of EB genotypes is the lack of visual cues to suggest the level of starch accumulation within the root. This inhibits breeding for EB as selection can only be accomplished through costly destructive methods. Taking this into consideration, there is a need for a non-destructive method to quantify cassava root development.

Cassava has many uses other than those provided by the roots. The leaves of the plant are high in crude protein (~ 25 %), and thus are often a valuable by-product for local farmers. After the transformation of the plant matter to silage to reduce the hydrocyanic acid to acceptable levels, it can be used to feed livestock (Nguyen et al., 2012). A recent study assessed the use of cassava silage as a feedstock for sheep in Indonesia (Sudarman et al., 2016). They found that feeding 20 % silage had a positive impact, similar to that of feeding the standard concentrate. It has been suggested that the formation of “cassava hay” through sun drying can produce a cattle

forage which, when supplemented, can potentially lead to improved yield and composition of the milk (Wanapat 2002). While the leaves are not the primary edible portion of the cassava plant, they are consumed as a food source. It is suggested that in the Congo the primary vegetable is the cassava leaf (Nweke et al., 2002). It is clear that increasing the amount of foliage produced would be desirable to local farmers and industries. To accomplish this, the selection of cassava genotypes which produce large quantities of high quality aboveground biomass is critical.

Phenotyping in cassava is generally done by hand, which is a laborious and time consuming task considering the size and long production cycle of the crop. The use of high-throughput phenotyping techniques could speed this process and reduce costs; however, little if any literature exists on the use of these type of techniques on cassava. Many phenotypic traits are of significance in the development of improved cassava genotypes. Cassava LAI and leaf retention have been suggested as important traits in the selection of drought tolerant genotypes (Okogbenin et al., 2003). Okogbenin et al. suggest that the ability of cassava to maintain leaf area under drought stress is linked to root yield potential. They also found that shoot biomass production was related to drought resistance, with the most resistant genotypes having little change across the drought regime. The study also suggested a correlation between root and shoot biomass might exist, but cautioned further study was required.

A group at the International Institute of Tropical Agriculture (IITA) produced a cassava descriptor list to help standardize the collection of important cassava traits (Fukuda et al., 2010). Within this document they propose the collection of height to first branching, branching habit, angle of branching and the overall characterization of the shape of the plant as important phenotypic measures. Other traits measured to assess cassava adaptation to drought stress include the number of primary stems, number of branching levels and the length of the primary

and secondary stems (Okogbenin et al., 2013). The authors noted the desirability of high shoot biomass in dry regions where the leaves are often used as a forage crop. They state the need for fast phenotyping protocols in the genetic selection of drought resistant cassava genotypes. Many of these desired traits might be measured using methods of high-throughput phenotyping described in other crop species

Phenomics

Phenomics is a discipline in the field of biology which is focused on the acquisition of phenotypic data on an organism-wide scale (Houle et al., 2010). The plant phenotype is the structural, physiological and performance-related expression of the plant as influenced by a gene, or more often a set of genes, in relation to the environment - also known as the gene by environment interaction (G x E) (Dhondt et al., 2013). Currently, our ability to understand the phenotypic state of a plant lags far behind our ability to describe its associated genotype. While many economically important crops have been genetically sequenced and annotated, the vast majority of these annotations lack the associated phenotypic functions (Furbank 2009). This fact has led many to describe phenotyping as one of the major bottlenecks to the future of crop development (Cabrera-Bosquet et al., 2012; Fiorani & Schurr 2013; Araus & Cairns 2014).

The main objective of plant phenotyping is to capture quantitative measures of a plant's response to the dynamic environment (Fiorani & Schurr 2013). The goal is to associate these data to the genotypic blueprint in order to develop a correlation between gene function, plant performance and environmental effects (Furbank 2009). However, many of the current methods of plant phenotyping are either costly, time-consuming, lack objectivity or are destructive (Montes et al., 2007; Busemeyer et al., 2013). Furthermore, the implementation of the current technologies has primarily been within a lab setting and thus lack the robustness needed for field

applications, especially in a high-throughput field phenotyping environment. This has led to the suggestion that the future of plant phenotyping should be a non-destructive and objective process (Fiorani & Schurr 2013). The need to develop methods which move past these issues has created a new push in the area of high-throughput phenotyping.

Current methods of plant phenotyping generally include the use of 2D image-based technologies such as broadband RGB and NIR, hyperspectral, fluorescence or thermal analysis. These techniques have been adapted from traditional satellite and aerial applications for field, greenhouse or laboratory use. In many cases these data are used to determine structural characteristics such as biomass, leaf area index (LAI), plant height or yield (Li et al., 2014). They can also be used to monitor biochemical features such as nitrogen status (Cabrera-Bosquet et al., 2011), plant water capacity (Elsayed et al., 2011) or plant stress (Lichtenthaler 1997) often with good results. In some cases, these 2D images have been extended to model the captured plant responses in 3D (Santos & Ueda 2013; Pound et al., 2014).

3D Phenotyping

The analysis of plants in 3D could allow a better understanding of morphological traits which have seen little investigation due to the historic need for extremely laborious manual acquisition (Dhondt et al., 2013). As a whole, the use of 3D data for phenotypic analysis is a relatively new venture; however, significant progress has been made since the turn of the century. The capture of 3D plant phenotypic data has been accomplished using several technologies. X-ray computed tomography (CT) and magnetic resonance imagers (MRI) have been used a to create 3D phenotypic plant data in specialized laboratories (Yang et al., 2011), while sonic digitizers have been used to capture high-resolution 3D data on plants within a laboratory (Watanabe et al., 2005) and in the field (Mack & Pyke 1979). However, this type of

technology is not often utilized for plant phenotyping because plant contact is required (Santos & De Oliveira 2012). As mentioned above, plants have been modeled through techniques such as stereoscopy, which use multiple 2D images and triangulation to produce 3D data. Stereo cameras tend to be low cost and offer high frame rates at the full spatial extent of the scene, which make them suitable for rapid temporal assessments. Depth cameras have also been used to capture 3D plant data (Klose et al., 2009; Chéné et al., 2012; Nguyen et al., 2015). They generally work either by using the time-of-flight principle or one based on structured light (Henry et al., 2014). These active sensors can be advantageous when the scenes have complex lighting and/or low texture (Du et al., 2011).

A large portion of 3D plant imaging is completed using laser ranging systems or what is often known as light detection and ranging (LIDAR) technology. In general terms, laser light is projected toward a target of interest and the time taken for the light to travel to the object and return is recorded. This information is used in conjunction with the sensor position to determine the object's location in 3D space. The field of Forestry has utilized airplane or helicopter-mounted LIDAR sensors to measure tree characteristics such as height and canopy diameter for several decades (Nelson et al., 1988; Popescu et al., 2003; Popescu 2007). This type of LIDAR is broadly known as aerial laser scanning (ALS), and has more recently been applied in agriculture (Anthony et al., 2014), though the mode of transportation for the platforms have shifted away from manned aircraft towards unmanned aerial vehicles (UAVs). Ground based laser ranging systems, known generally as terrestrial laser scanners (TLS), have been used extensively to measure plant characteristics. TLS have been used widely to quantify the aboveground structure of forest (Litkey et al., 2008; Hackenberg et al., 2015) and agronomic species (Eitel et al., 2014; Tilly et al., 2014).

Terrestrial Laser Scanning

Terrestrial laser scanners have the ability to record fine details of an object in 3D. Many scanners are able to record reflective properties of the object's surface, which relates to the wavelength of the laser and the distance and incidence angle to the object. Some scanners include built-in RGB cameras, which can be used to colorize the pointcloud. Laser scanners work by pulsing laser light, often at a single wavelength, at an object and use the time-of-flight and speed-of-light to determine the distance. This distance measure, along with the horizontal (azimuth) and vertical (zenith) angles between the instrument and the object, are recorded for each laser pulse. This information is used to perform simple trigonometric calculations to create a 3D pointcloud of the object. The pointclouds from multiple scans captured around the object can be registered together and information related to the reflectance and color images can be applied to form a data-dense 3D representation.

Terrestrial laser scanners have been used to further many fields of study. While the majority of commercial units are sold to conduct architecture and engineering surveys, many have been used to conduct studies in other fields such as geology (Buckley et al., 2008), forestry (Watt & Donoghue 2005) and archaeology (Lerma et al., 2010). Within the field of agriculture, TLS has been used to characterize several important phenotypic and environmental traits. Aboveground biomass determination has been conducted in many species including oilseed rape (*Brassica napus*), winter rye (*Secale cereale*), winter wheat (*Triticum aestivum*), grassland (Ehlert et al., 2008; Ehlert et al., 2009; Ehlert et al., 2010) and vineyard (Keightley & Bawden 2010) studies with significant results.

Terrestrial laser scanners have been used to look at crop growth across time, detect the location of individual plants and assess the field environment. Temporal measures of crop

growth variability across a field have been conducted with both sugar beet and barley (Hoffmeister et al., 2016). Short duration growth-related changes in canopy height in several species was discernable, with maize growth detectable within a few hours (Friedli et al., 2016). Individual early stage plant detection in maize was possible using a full-waveform TLS and radiometric correction (Höfle 2013). Hydrology is a key component of the within field variability in crop growth, and is driven in part by the topography. The micro-topography of agricultural watersheds has been assessed using a combination of TLS and UAV-based photogrammetry (Ouédraogo et al., 2014). Additionally, soil roughness in a crop field was characterized with a TLS in hopes of being used as ancillary data for soil moisture analysis via synthetic aperture radar (Perez-Gutierrez et al., 2007).

Terrestrial laser scanners have been used to estimate the leaf area of several crop species. A tractor-mounted laser scanner was used to estimate leaf area of grapevines in a vineyard (Arnó et al., 2013). A modified laser scanner was used to create polygons to represent the individual leaves of a tomato plant (Hosoi et al., 2011). A similar result was found in wheat, where leaf area density (LAD) and plant area density (PAD) were estimated across different growth stages (Hosoi & Omasa 2009). TLS have been used to assess nitrogen and chlorophyll content in several species of agricultural crops. Measurement of laser-induced chlorophyll florescence (LICF) was conducted on winter oilseed rape (*Brassica napus L.*) using a ratio of two wavelengths, 690 and 730 nm (Thoren & Schmidhalter 2009). In a field study of spring wheat (*Triticum aestivum* L.) a TLS was used to assess foliar nitrogen status during stem elongation (Eitel et al., 2011). In another paper on spring wheat, a laser scanner was used to assess nitrogen status across 2 different seasons at both tillering and jointing (Eitel et al., 2014).

To the author's knowledge, no literature exists on the use of terrestrial laser scanners, or LIDAR in general, on cassava. However, some remote sensing studies have been published which use satellite imagery to assess the crop. Data from the NOAA-14 satellite was combined with topography and land use data to map the cassava plantation area in the northeast region of Thailand (Eiumnoh & Shrestha 1999). Images from the Advanced Land Observation Satellite (ALOS) were used to develop a method to characterize the spatial-temporal distributions of cassava fields in northeastern Thailand (Yoshida & Nagasawa 2010). Images from two different satellites were used to determine the plantation area of cassava in the Siracha district, Chonburi province of Thailand (Kruasilp & Rungsipanich 2010). They used fuzzy logic and object-oriented classification to overcome some limitations of the previous pixel-based techniques.

Depth Sensors

In recent years, depth sensors have seen significant advancement due in large part to robotics and computer vision applications. These types of sensors are used in a broad array of fields for things such as robotic navigation, object reconstruction, human computer interaction (Zhu et al., 2008) and even surgical applications (Tanner 2000). There are several types of sensors which fall into the depth sensor category, including passive sensors (that use stereo-vision) and active sensors (which project light into the scene to determine depth).

Active depth sensors work on two basic principles: structured light or time-of-flight. Structured light sensors work by projecting a structured light pattern onto the scene and capturing the reflected light through the use of a separate camera. The deformation of the light pattern is used to calculate the spatial position of each of the pixels captured by the camera. In general, this yields a 3D pointcloud which is often further colorized by information from the camera (Rocchini et al., 2001). Time-of-flight sensors function by measuring the time-of-flight

of a signal sent from the sensor to the object and back to the sensor. The signal source would generally be light, though sound or radar are also used (Gokturk et al., 2004_a). The time-of-flight sensor uses a modulated light, such as a laser, along with a sensor for detecting the light once it has been reflected (Gokturk et al., 2004_b). Two principles are generally used to determine the time estimation: pulsed or continuous wave modulation. In pulsed modulation, the time taken for the light to leave the laser, reflect of an object and return is used along with the speed of the light to determine distance. In continuous wave modulation, the phase shift between the emitted light and an internal control are used to determine distance (Horaud et al., 2016).

Depth sensors have been utilized in a broad array of fields. For example, they have been used in human biometrics, where these sensors can determine hand gestures (Kurakin et al., 2012) and other human actions (Chen et al., 2015). Depth sensors have even been used for biometric determination in other species, such as in detecting pig aggression (Lee et al., 2016). Aside from biometric studies, depth sensors are utilized for such tasks as navigation of autonomous vehicles (Eric and Jang 2017) as well as to assist the visually impaired (Kanwal et al., 2015).

Depth sensors have been studied for applicability as a phenotyping tool in an agricultural context. The comparison of several active time-of-flight sensors against a passive stereo-based 3D imaging platform was performed to test both indoor and outdoor leaf phenotyping performance (Kazmi et al., 2014). A robotic arm was guided by a time-of-flight sensor to perform leaf segmentation and extract disc samples for further analysis (Alenyà et al., 2013). Maize plants were reconstructed using a time-of-flight sensor mounted to an autonomous robot developed at the University of Hohenheim (Vázquez-Arellano et al., 2018). Depth sensors were

even combined with other sensors to produce a multi-sensor phenotyping platform designed for small grain cereals, which was tested on triticale (*Triticosecale Wittmack L.)*.

However, depth sensors do have limitations. Stereo cameras, while they operate well under varying light conditions, are often limited in range and perform poorly when the scene has low texture (Gutierrez and Marroquin 2004). Structured light sensors are limited by motion blur when used in dynamic scenes, an issue derived from the inherent lower framerates. In addition, optical interference is a problem for structured light sensors and therefore they are best suited for indoor environments (Li 2014). Time-of-flight sensors are not without their limitations. Most commercially available sensors perform poorly in bright sunlight, an issue related to the energy output from the diode being washed out. In addition, time-of-flight sensors are susceptible to "flying pixels," which are caused by depth measures which occur on the edge of object and return two distance values. Subsequently, these two values are averaged and thus a depth measure somewhere between the two surfaces is returned (Butkiewicz 2014).

Microsoft Kinect

The Microsoft Kinect V1 sensor was introduced in 2010 for use with the Xbox 360 gaming console. In 2011, a software development kit (SDK) was released, allowing it to be used by researchers as a low-cost 3D sensor (Anderson et al., 2012). The Kinect V2 sensor released in 2014, was the second depth sensor released by Microsoft for use with its Xbox One console. The Kinect V2 sensor is cited often in recent literature due its wide availability, low-cost and good performance. Unlike the V1 sensor, which uses the structured light modality, the V2 sensor utilizes the time-of-flight principle, and in general is a step ahead of the original version. The Kinect V2 utilizes the continuous wave modulation method of depth estimation. It has a depth resolution of 512 X 424 pixels and a RGB color resolution of 1920 X 1080. The sensor operates

at a maximum of 30 fps, which is adjusted to 15 fps in low light. The depth image is operable from ~ 0.5 to 4.5 m (Corti et al., 2016).

The Microsoft Kinect V2 has been used for a wide range of applications including: 3D modeling (Lachat et al., 2015_a), head motion tracking (Noonan & Hallett 2015), kinematic gate assessments (Geerse et al., 2015) and coastal mapping (Butkiewicz 2014). In addition, the Kinect V2 sensor has been used in several studies related to the field of agriculture. For instance, the sensor was used to predict cotton plant height in both a lab and field setting (Jiang & Paterson 2016). The Kinect V2 was mounted to an autonomous robot to allow 3D reconstruction of maize plant rows in a greenhouse (Vázquez-Arellano et al., 2018). The identification of weeds within a maize field was conducted with the sensor with great success (Andújar et al., 2016). The sensors have even been mounted to robots within a growth chamber, to allow complete real-time segmentation of plants (Shah et al., 2016).

CHAPTER IV

PREDICTING CASSAVA HEIGHT USING A TERRESTRIAL LASER SCANNER UNDER FIELD CONDITIONS

Introduction

Cassava (*Manihot esculenta*) is the sixth major staple crop in the world (Mann 1997). It is grown across the tropical and subtropical regions where it provides food for 800 million people worldwide (Prochnik et al., 2012). Within sub-Saharan Africa in 2008, over one hundred million tons of cassava was produced, placing it above maize in total production (Sayre et al., 2011). Within Latin America and the Caribbean cassava plays a dual role in food security and as a feedstock, while in Asia it has become an important industrial crop. Considering the worldwide importance of cassava, especially within developing countries, it is assumed that yield improvements would strengthen economic growth within these areas through the transition of cassava from a subsistence to a cash crop (Nassar & Ortiz 2007).

A group at the International Institute of Tropical Agriculture (IITA) produced a cassava descriptor list to help standardize the collection of important cassava traits (Fukuda et al., 2010). Within this document they propose collecting height to first branching, branching habit, angle of branching and the overall characterization of the shape of the plant as important phenotypic measures. Many of these desired traits might be measured using methods of high-throughput phenotyping described on other crop species. Phenotyping in cassava is generally done by hand, which is a laborious and time consuming task considering the size and long production cycle of the crop. The use of high-throughput phenotyping techniques could speed this process and

reduce costs, however little, if any, literature exists on the use of these types of techniques on cassava.

Height is an important predictive trait in many agricultural crops (Freeman et al., 2007; Pask et al., 2012), and is often one of the first to be explored in a high-throughput phenotyping context (Zhang & Grift 2012; Holman et al., 2016). In cassava, height is considered a major architectural trait (Okogbenin et al., 2003) and is often used as a descriptor for pest susceptibility (Byrne et al., 1982), as well as an indicator of environmental stress (Connor & Cock 1981).

The terrestrial laser scanner is one tool which has been used to predict plant height in several crops. TLS have the ability to record fine details of an object in 3D. Many scanners are able to record reflective properties of the objects surface which relates to the wavelength of the laser and the distance and incidence angle to the object. Some scanners include built-in RGB cameras which can be used to colorize the pointcloud. Laser scanners work by pulsing laser light, often at a single wavelength, at an object and use the time-of-flight and speed-of-light to determine the distance. This distance measure, along with the horizontal (azimuth) and vertical (zenith) angles between the instrument and the object, are recorded for each laser pulse. The collected information is used to perform simple trigonometric calculations to create a 3D pointcloud of the object. Pointclouds from multiple scans captured around the object can be registered together, and information related to the reflectance and color images can be applied to form a data dense 3D representation.

Terrestrial laser scanners have been used to further many fields of study. While the majority of commercial units are sold to conduct architectural and engineering surveys, many have been used to conduct studies in other fields such as geology (Buckley et al., 2008), forestry (Watt & Donoghue 2005) and archaeology (Lerma et al., 2010). Within the field of agriculture,

TLS has been used to characterize several important phenotypic and environmental traits with significant results (Perez-Gutierrez et al., 2007; Ehlert et al., 2008; Ehlert et al., 2009; Ehlert et al., 2010; Keightley & Bawden 2010). Specifically, plant height has been characterized across several species using a TLS. Field-level growth of sugar beets (*Beta vulgaris*) and winter barley (*Hordeum vulgare*) was captured over time using a TLS-derived canopy height model (Hoffmeister et al., 2016). Growth over time in maize (*Zea mays*) soybean (*Glycine max*) and wheat (*Triticum aestivum*) were all predicted using height analysis with a TLS (Hoffmeister et al., 2010). Plant height has also been predicted in paddy rice (*Oryza sativa*) using this technology (Tilly et al., 2013).

As a first step towards the development of a high-throughput phenotyping tool for cassava, we attempted to predict the height of three genotypes of cassava in a field setting using the Trimble® TX5 (Trimble Inc. Sunnyvale California) terrestrial laser scanner.

Methods

Location and Study Design

The field site was located at the International Center for Tropical Agriculture (CIAT) near Cali Colombia (Figure 1). Cassava cuttings of three different genotypes, which contrasted in their growth pattern, were planted on raised rows in early January of 2018. Genotype 1 (GM3893-65) is considered an asparagus genotype as it is tall and slender, Genotype 2 (CM523-7) is an erect type with most of its vegetation near the canopy with little branching, while Genotype 3 (MPER-183) is a shrub type with much branching and vegetation near the ground as well as in the canopy. Four plots of each genotype were planted in a block, with each plot containing 5 rows and 9 plants per row (Figure 1). A blank space of 2 meters was created between each 5th row to separate the plots, while a buffer of 2 plants was grown to separate the 3

blocks. A buffer of 2 plants was also grown at the beginning and end of each row, and a single row buffer was planted as the first and last rows of the trial. This resulted in each row containing 35 total plants with a total of 21 rows. All of the plants received the same treatment of fertilizer, with select individual plants receiving treatments of insecticide, to promote proper growth.

Field Measurements

In mid-April of 2018, height for each plant was determined manually using a measuring stick. The estimation was determined from the top of the hill plot to the highest point on each plant. A conservative estimation of the error in these measurements is predicted to be ± 3.0 cm. This error is mainly derived from the placement of the measuring stick on the varying topography of the hill plots.

TLS Scans

The following morning, TLS scans were captured of the entire study using a Trimble TX5 3D terrestrial laser scanner. The sensor has a range of 0.6 to 120 m with a ranging error of ± 2 mm at 10 m & 25 m and operates at 905 nm. During the scanning period winds were light and variable, causing some movement in the leaves of the cassava plants. The scan locations and sensor parameters were chosen to maximize coverage of the field while minimizing the time required to capture the data. A total of 8 scans were captured (Figure 1). Four scans were captured from the 4 outside corners of the experiment. Two scans were taken along the east and west perimeters of the field adjacent to the blank area which separated the middle two plots. The last 2 scans were captured from the interior of the study from within the blanks which separated the 1st and 2nd, and 3rd and 4th, plots. These two scans were offset in an east-to-west fashion to provide better coverage.

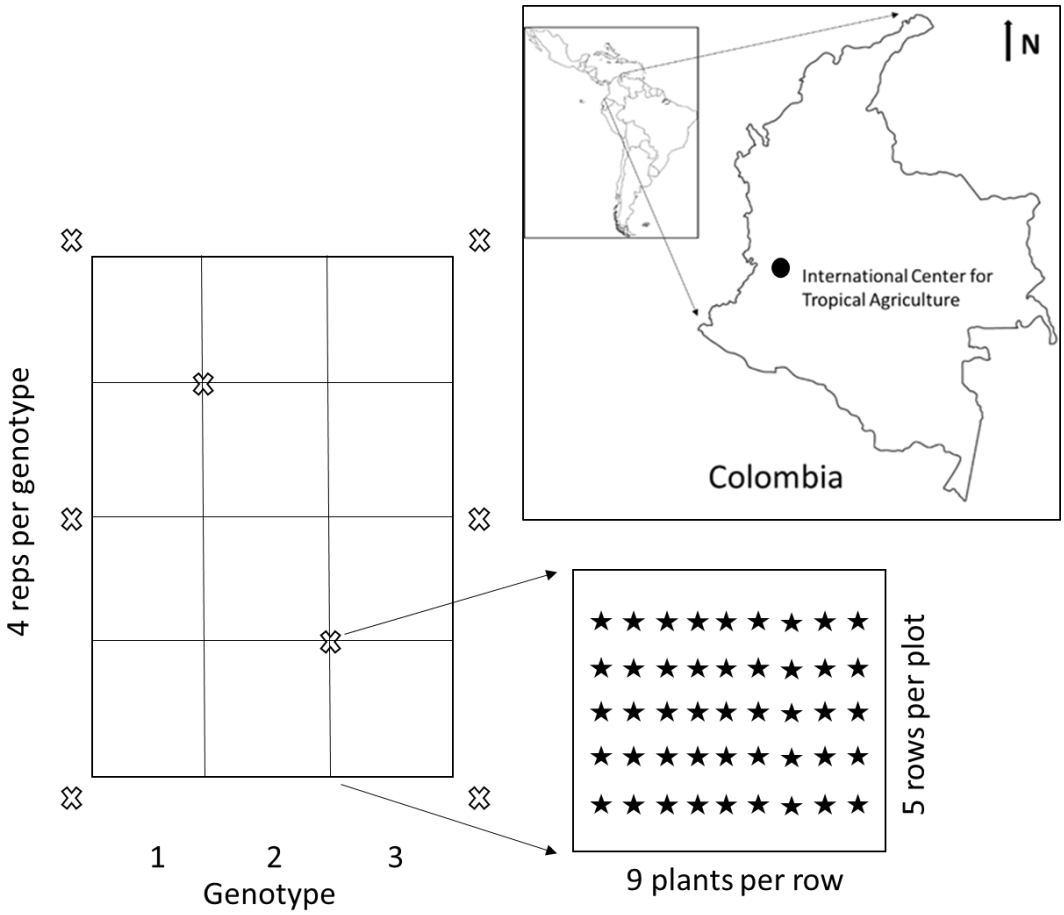

Figure 1. Field location, 8 scan locations and plot map. A circle represents the location of the International Center for Tropical Agriculture. The X's represent the scan locations. Stars represent the individual plants in a plot.

Eight 360° scans were captured using the maximum scan area of the scanner (vertical from -60° to 90° and horizontal from 0° to 360°). The scanner was set to capture at a point spacing of 7.67 mm at 10 m from the scanner. The scan parameters were set to a "resolution" of 1/5 and a "quality" of 3X. Color photos were also captured by the scanner at the end of each scan cycle in order to aid in manual registration and identification of artifacts in the pointcloud. This resulted in a time of approximately 6 ½ minutes per scan location. The scanner was mounted on a professional survey tripod and was set to a height of approximately 1.5 m for each scan.

Pointcloud Processing

The first step in the data analysis process was to open each scan in the Trimble's SCENE software and export each as a .txt file. No manipulation of the data was conducted before exporting from SCENE. We used LAStools (LAStools 2014) and the "txt2las" tool to convert each scan from the .txt to .las format. At the time of this publication the SCENE software did not offer export in this format.

We used CloudCompare (CC), an open-source 3D data analysis and visualization software, to complete the registration process (CloudCompare 2016). Each of the scans were registered together using "targets" or known common points between the scans, which were available in the field. Registration accuracy was determined visually, assuring known objects were in alignment between the scans. Wooden stakes, which marked plot rows, were used along with other stationary markers for this task. Scan registration order was such that those which were closest together where done first. In order to eliminate duplicate points in the registered pointcloud, the "remove duplicate points" tool in CC was used with a minimum distance between points set to 2 mm. This distance was chosen as this is the minimum resolution of the Trimble TX5. The removal of these points cut down on the data storage and processing requirements with little to no degradation in the pointcloud accuracy.

Normalization of the data was conducted to standardize the height of the scan points based on the ground points below. The field area, with a small buffer to allow accurate kriging, was segmented out of the registered pointcloud using the "segment" tool in CC. For the rest of the normalization process we used the "lidR" package in R (R core team 2013). The "lasground" tool was used to classify the ground points across the field. The tool uses a loose implementation of the Progressive Morphological Filter (PMF) credited to Zhang et al. (2003). The maximum

window size was set to 1.0 m and the height threshold was set to 0.2 m. We determined these values by trial-and-error and visual assessment of the results. The "grid_terrain" tool was used to create a digital terrain model using the classified ground points. The interpolation was completed using the "kriging" method which in this case uses universal kriging. The number of nearest neighbors was set to 10. Finally, the "lasnormalize" tool was used calculate the height aboveground for each point where the ground below was set to a height of 0.

Each plot was visually segmented out of the field level pointcloud using the "segment" tool in CC and saved as a unique file. Care was taken to not include the buffer plants in any of the plots. From this point all processing was done on a plot-by-plot basis. The "SOR filter" (Statistical Outlier Removal) in CC was used to clean-up much of the noise. The settings were determined by trial-and-error and visual assessment of the resulting pointcloud. The settings used were 6 for the number of nearest neighbors and 1.00 for the standard deviation multiplier. Each plot was visually assessed for remaining noise points and any obvious ones were manually removed using the "segment" tool in CC. These were mainly random points above the canopy layer and between the rows of plants. Additionally, any wooden markers were manually removed.

Semi-automated identification of individual plants and determination of their height was the main goal. To accomplish this, a combination of the R package "lidR" and CC were used. The first step was to remove the ground points which were previously classified. To accomplish this, each plot file was opened in CC and the "filter points by value" tool was used. In order to classify individual plants within the plot, the "lastrees_li2" function within the "lidR" package was used. This function performs an individual tree segmentation using the algorithm described in Li et al. (2012) and assigns unique tree ID values to each point in the dataset. The function

works on the pointcloud level, which is ideal for this application. The algorithm in "lidR" has the addition of a parameter "hmin" which sets the minimum height of a detected tree. This was added to stop over-segmentation of objects which are too low. The arguments for the "lastrees_li2" function were set based on a trial-and-error approach for each genotype of cassava being assessed (Table 1). The two values "dt1" and "dt2" are the two threshold distances used. The recommended value for dt1 is that of the crown diameter. The threshold value of dt1 is used unless the elevation of the point is above the value assigned by "Zu," in which case the value of dt2 is used. The principle here is to use an adaptive threshold, as trees which are taller should have a greater crown diameter than those of shorter trees. The value "R" assigns the search radius for the local maxima. If a value of 0 is assigned, all values are considered. The last value is "speed-up" which affects the processing speed. The authors of the function suggest any value that is greater than the crown diameter will not affect the result, but the smaller the value, the quicker the processing.

Table 1. lastrees_li2 arguments.

	Assigned Value (in units of pointcloud)		
Argument	Genotype 1	Genotype 2	Genotype 3
dt1	.3	.5	.5
dt2	.4	.7	.7
R	0	0	0
Zu	.5	1.0	1.0
hmin	.2	.2	.2
Speed_up	2	2	2

Once the segmentation of individual trees was complete, the “metrics” function within “lidR” was used to determine the maximum height of each tree identified in the segmentation process. These data were output as a .txt file, which included the unique tree ID and associated tree heights.

The assignment of unique tree ID values during the classification process was based on the processing order and cannot be assigned to match the field map. Thus, each classified pointcloud was opened in CC to complete this cross-reference manually. The “point picking” tool was used to display each unique tree ID value and this value was matched to the field map based on its position in the field. These cross-referenced values were added to the original field data along with the LIDAR derived height data using Microsoft Excel.

Many of the plants were not visible or were poorly represented (only a few sporadic points existed where the plant should have been) in the scans, which can be attributed to three

main factors: 1) The height of the scanner was at or below many of the larger cassava plants which blocked them from view. 2) The large distance from the scan positions to some of the plants meant that several rows of plants were often between them and the scanner. 3) The scans were captured when winds were moving some of the cassava leaves, which may have increased the shadowing effect. Because of this, any plants which were not visible or poorly represented in the scans were removed from the primary dataset.

Some of the plants, especially for Genotype 3, were not classified correctly, which led to the creation of a corrected dataset. The main cause of this was a combination of the poor representation of some of the plants, along with the overlapping canopies of a few of the large cassava plants. To combat this, the manual removal of points between the plants with overlapping canopies was conducted using the "segment" tool in CC. The classification algorithm was again run on these new data to produce the corrected dataset. During the cross-reference step those plants which were not visible in the scans were also removed from these data.

Analysis

A series of regression analyses to test the ability of the LIDAR-derived height to predict the field measured height were conducted in R. These were conducted on a genotype-by-genotype and entire-field basis, both using the primary and corrected datasets. A field-level assessment was conducted with both the primary and corrected datasets, while only the corrected dataset was used in the by-genotype analysis.

Results

The primary dataset, which included all of the plants except those which were not visible or poorly represented in the scans, was regressed against the hand-collected field height data (Figure 2). The result was an R^2 of 0.65 with a P-value of 2.2e-16.

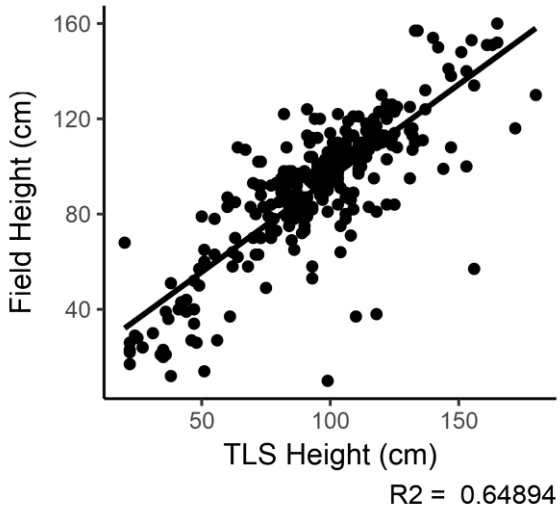

Figure 2. Field-level analysis of the primary dataset (n = 288).

For the corrected dataset, both field-level and by-genotype regression analyses were conducted. The corrected dataset included further manual manipulation of the pointclouds, as well as the removal of plants which were not visible in the scans. For the field-level assessment the R^2 was 0.81 with a P-value of 2.2e-16 (Figure 3). On a by-genotype basis, the LIDAR derived height data correlated best with the field height measures for Genotype 2 (Figure 4). The

R^2 value was 0.9 with a P-value of 2.2e-16. Genotype 1 had an R^2 value of 0.88 and a P-value of 2.2e-16, while the worst performer was Genotype 3 with an R^2 of 0.51 and a P-value of 1.06e-14.

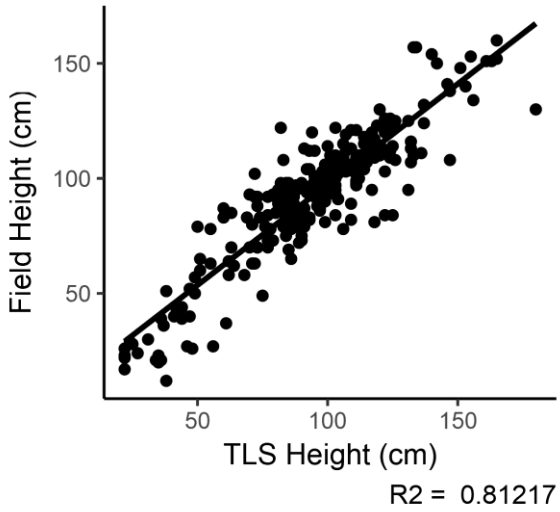

Figure 3. Field-level regression of the corrected dataset (n = 260).

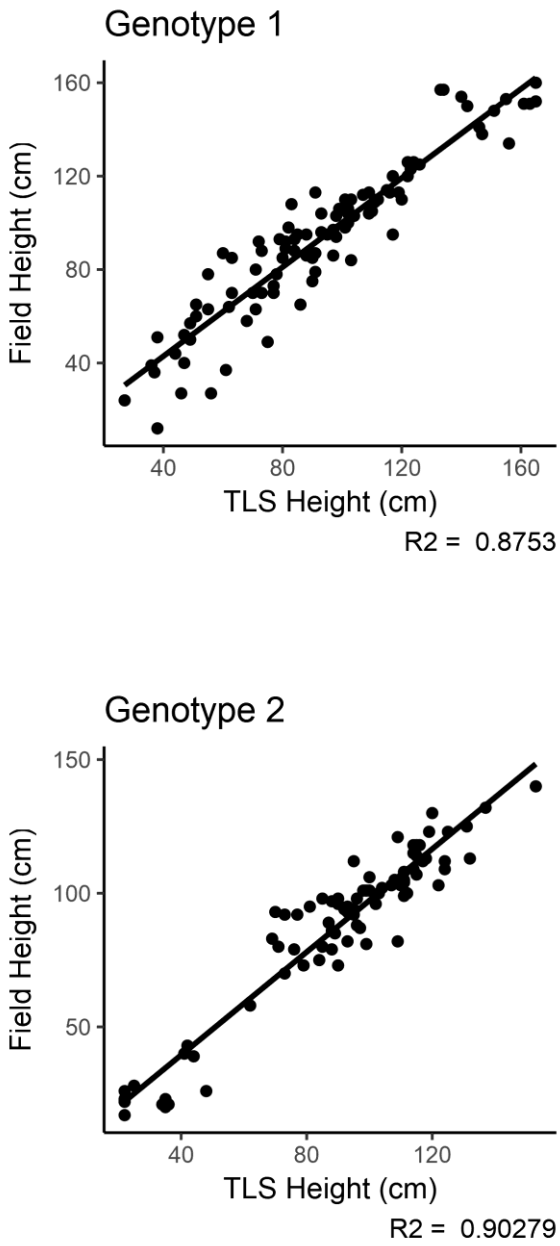

Figure 4. By-genotype analysis of the corrected data; all three genotypes shown (Genotype 1 n = 95; Genotype 2 n = 80; Genotype 3 n = 83).

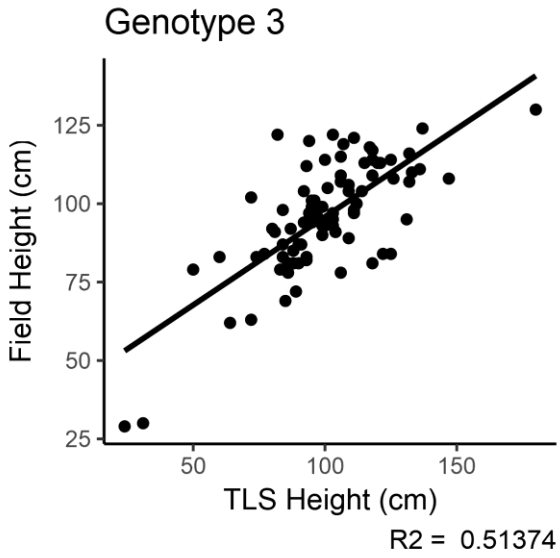

Figure 4. Continued.

Discussion and Conclusions

In this study, a well-known tree classification algorithm by Li et al. (2012) was used in an attempt to automate the classification of individual cassava plants in a field for height determination. The results of the regression analysis which stemmed from this classification were merely satisfactory (R^2 = 0.65; P-value = 2.2e-16) when the scan data included overlapping canopies. Many plants, especially in Genotype 3, had an overlapping canopy structure. This caused them to be wrongly classified, leading to substantial errors in height estimation. When manual removal of the overlap within those canopies was conducted, the ability of the TLS to predict cassava height increased (R^2 = 0.81; P-value = 2.2e-16). However, this manual removal process is somewhat subjective and rather time consuming. The methodology presented here was more successful at predicting cassava height when separation between the canopies existed

(Genotype 1 R^2 = 0.88; P-value = 2.2e-16 & Genotype 2 R^2 = 0.9; P-value = 2.2e-16). The lack of canopy overlap with these two genotypes, along with the reduction in shadowing (especially with the asparagus type), resulted in better individual plant representation and classification.

Depending on the level of predictability required, the use of minimal field-level scans during relatively calm weather, combined with the semi-automated analysis process described here, could allow rapid height determination of the asparagus or erect-type cassava genotypes. Improved results of height prediction might be achieved, especially for shrub-type genotype, through the implementation of a few changes to the scanning methodology. First, raising the height of the scanner above the maximum canopy height and capturing more scans per plot should reduce the shadowing effect at thus improve individual plant scan quality. In addition, capturing the scans during a period with as little wind as possible would also improve scan quality. However, these techniques might not have a powerful effect on the segmentation of plants with overlapping canopies.

The automated segmentation of individual plants is a complicated task, especially when overlap exists between them. In the case of individual plant height estimation, this might be overcome through the use of referenced plant locations. The methodology used here could be applied on juvenile plants prior to the overlapping of canopies, thus allowing the proper classification and identification of the plants. Their position information could then be applied to future scans as the canopies closed, avoiding any classification issues. Another approach might be the classification of individual plants based on the identification of their primary stalks. This might be possible with the higher resolution scans discussed earlier.

The last major issue with this methodology is the assignment of Tree ID values by the classification tool. The “lidR” methodology seems to assign Tree ID values based on the

processing order from largest to smallest Z value, which does not match the typical row-by-row plant identification scheme of agricultural fields. A raster-based solution, which associates the field ID's to those derived from the classification tool, might automate this process.

There is a strong need for high-throughput phenotypic analysis in cassava, however, little work has been done to date. TLS has proven to be a strong candidate as a predictor of plant height in many agricultural crops, though to the author's knowledge no one has demonstrated this on cassava in a field setting. Our results suggest that the TLS can be used to predict the height of individual cassava plants in a field environment using just a few scans and a semi-automated analysis process. However, as the canopies start to overlap, whether due to planting density, age, or varietal growth characteristics, the accuracy of individual plant classification, and thus the predictive power, will decrease. There is a strong need for further research into the ability of TLS and other methods of 3D modeling to predict structural characteristics of interest in cassava, including height to first branching, branching angle and overall characterization of plant shape.

CHAPTER V

PREDICTION OF ABOVEGROUND BIOMASS OF THREE CASSAVA GENOTYPES USING A TERRESTRIAL LASER SCANNER

Introduction

Cassava (*Manihot esculenta*) originated in South America and was first cultivated between 4,000 and 2,000 B.C. However, it has only recently become a global crop (Fauquet & Fargette 1990). It is estimated that over 13 million hectares of cassava are cultivated annually, and its yield is used primarily as a source of carbohydrates and secondarily as animal feed. The crop is grown in such quantities due to its ability to thrive in marginally fertile soils and under various rainfall conditions (El-Sharkawy 2003). In addition to its hardy nature, cassava also tends to out preform many other tropical staple crops on a per-hectare energy yield basis, leading to its widespread use across much of the tropics (Montagnac et al., 2009).

Considering the worldwide importance of cassava, especially within developing countries, its assumed that yield improvements would strengthen economic growth within these areas through the transition of cassava from a subsistence to a cash crop (Nassar & Ortiz 2007). Late bulking has been described as the single cause for rejection of genotypes in sub-Saharan Africa (Nweke et al., 2002). This has led many to attempt to improve yield and promote early bulking (EB) within the roots (Okogbenin & Fregene 2002; Ceballos et al., 2004). It has been suggested that breeding for EB genotypes would have two significant advantages: a shortening of crop duration and increased yield (Okogbenin & Fregene 2002). The main roadblock to the development of EB genotypes is the lack of visual cues to suggest the level of starch accumulation within the root. This inhibits breeding for EB, as selection can only be

accomplished through costly destructive methods. Taking this into consideration, there is a need for a non-destructive method to quantify cassava root development.

Cassava has many other uses other than those provided by the roots. The leaves of the cassava plant are high in crude protein (~ 25 %), and thus are often a valuable by-product for local farmers. After the transformation of the plant matter to silage, to reduce the hydrocyanic acid to acceptable levels, it can be used to feed livestock (Nguyen et al., 2012). A recent study assessed the use of cassava silage as a feedstock for sheep in Indonesia (Sudarman et al., 2016). It found that feeding 20 % silage had a positive impact similar to that of feeding the standard concentrate. It has been suggested that the formation of "cassava hay" through sun drying can produce a cattle forage which, when supplemented, can potentially lead to improved yield and composition of the milk (Wanapat 2002). While the leaves are not the primary edible portion of the cassava plant, they are consumed as a food source. It has been said that in the Congo the primary vegetable is the cassava leaf (Nweke et al., 2002). It is clear that increasing the amount of foliage produced would be desirable to local farmers and industries. To accomplish this, the selection of cassava genotypes which produce large quantities of high-quality aboveground biomass is critical.

Phenotyping in cassava is generally done by hand, which is a laborious and time-consuming task considering the size and long production cycle of the crop. The use of high-throughput phenotyping could speed up this process and reduce costs; however, little if any literature exists on the use of these type of technique on cassava. Many phenotypic traits are of significant importance in the development of improved cassava genotypes. Cassava leaf area index (LAI) and leaf retention have been suggested as important traits in the selection of drought-tolerant genotypes (Okogbenin et al., 2003). Okogbenin et al. suggest the ability of

cassava to maintain leaf area under drought stress is linked to root yield potential. They also found that shoot biomass production was related to drought resistance, with the most resistant genotypes having little change in leaf retention across the drought regime. The study also suggested a correlation between root and shoot biomass might exist, but cautioned further study was required.

Terrestrial laser scanners have the ability to record fine details of an object in 3D, and often capture additional data such as intensity or RGB images. Many scanners record intensity, or the reflective property of the object's surface, which relates to the laser wavelength as well as the distance and incidence angle to the object. In addition, some scanners include built-in RGB cameras which can colorize the pointcloud.

Laser scanners work by pulsing laser light, often at a single wavelength, at an object and use the time-of-flight and speed-of-light to determine the distance. This distance measure along with the horizontal (azimuth) and vertical (zenith) angles between the instrument and the object are recorded for each laser pulse. This information is used to perform simple trigonometric calculations to create a single point in 3D space, which when combined with other points forms a pointcloud. The pointclouds from multiple scans captured around the object can be registered together and information related to the reflectance and color images can be applied to form a data-dense 3D representation.

To the author's knowledge, no literature exists on the use of TLS, or LIDAR in general, on cassava. However, they have been used to assess phenotypic characteristics of many other crops. TLS can be used to conduct temporal measures of crop growth (Hoffmeister et al., 2016), allow for early stage plant detection (Höfle 2013) and predict plant area (Hosoi & Omasa 2009). Aboveground biomass determination has been conducted in many species including oilseed rape

(*Brassica napus*), winter rye (*Secale cereale*), winter wheat (*Triticum aestivum*) and grasslands (Ehlert et al., 2008; Ehlert et al., 2009; Ehlert et al., 2010). Vineyard studies have also been conducted with significant results (Keightley & Bawden 2010).

As a preliminary step toward the use of high-throughput phenotyping in cassava breeding, we attempted to use a Faro Focus 120 TLS (Faro Technologies Inc., Laker Mary, USA) to predict several categories of aboveground biomass in 3 genotypes of cassava which differed in their aboveground structure. Our goal was to use TLS data to predict biomass of the entire plant, as well as the biomass within specific height bins. The bins chosen were 20 cm in height, and were initiated from the base (where the primary stalk meets the soil) and extended to the top (the upper most leaf) of each plant. Two weight categories per height bin were created: 1) the dry weight of the leaves and 2) the combined stalk(s) & stems weights. In addition to the binned height assessment, we summed the weight categories for each plant to obtain a total leaf dry weight, a total stalk & stem dry weight as well as a total plant dry weight. Analysis was done across the 3 genotypes, as well as between them, in order to assess any limitations of the LIDAR data with specific plant structures. Specifically, we tested several LIDAR data processing approaches, to identify the best practices for using LIDAR data as a predictor of several measures of biomass for 3 contrasting genotypes of cassava. One of these approaches included testing the feasibility of using single scans versus two registered scans of each plant to correlate to the various biomass measures.

Methods

The experiment was initiated in the winter of 2016 at the International Center for Tropical Agriculture (CIAT) (Figure 5). Three genotypes of cassava were chosen based on their contrast in aboveground structure (Figure 6). Genotype 1 (CM523-7) is a typical erect shrub type

cassava with few erect branches initiating above the ground surface. Genotype 2 (GM3893-65) is known as an asparagus type with its characteristic lack of branches and its leaves which grow directly from the main stalk. The genotype allows a higher planting density due to its very erect growth structure. Genotype 3 (HMC-1) is another shrub type, but it has a lower branching structure with braches often running near to the ground surface. While both shrub types, Genotype 3 has a much lower growth pattern than that of Genotype 1.

Planting began in December of 2016, with subsequent plantings taking place approximately each month through August of 2017. The planting was done in a staggered fashion to allow data on all 9 age groups to be collected at one time (Figure 7). This resulted in 9 age groups, from 3 to 11 months of age, during the data collection period in November of 2017. The age groups were created to produce variability in the biomass of each genotype. For each planting, 15 plants of each genotype were planted from cuttings into a 3 plant by 5 plant plot. The spacing between plants, as well as between rows, was 1 m. This exaggerated spacing was used to reduce the overlap between the plants, as well as to facilitate an unrelated phenotyping study which will not be discussed here. A double border was planted around the entire experiment, but no border was used between plots. The experiment received irrigation, fertilizer and any necessary pest treatments required to maintain normal growth.

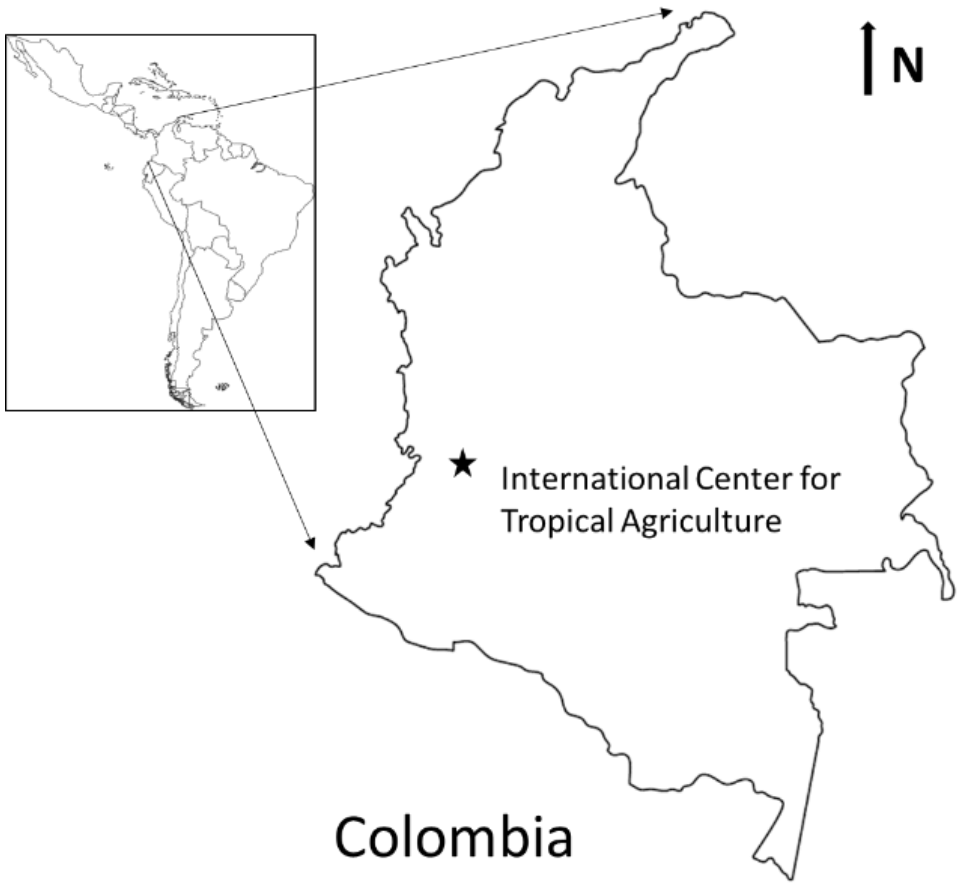

Figure 5. Location of the International Center for Tropical Agriculture. Approx. 16 km East, North East of Cali Colombia. Location of the research center is represented by a star.

Figure 6. Examples of the 3 cassava genotypes used in the study. 1) Erect shrub type (523-7), 2) asparagus type (Esparrago), & 3) low branching type (HMC-1).

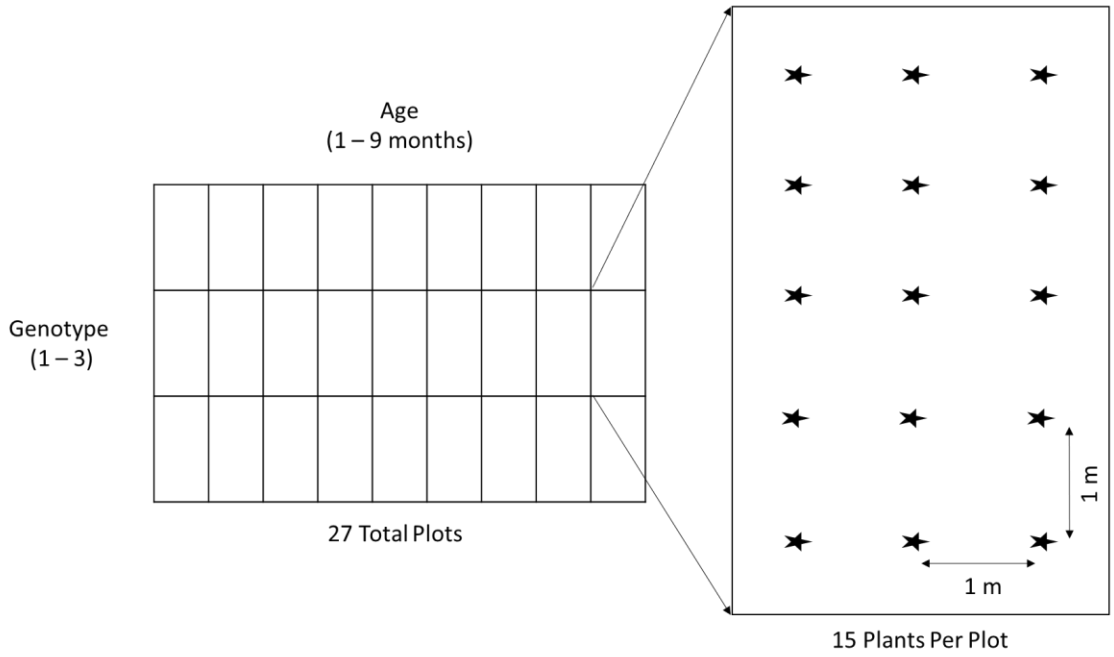

Figure 7. Planting map. With 9 age groups, 3 genotypes (27 plots) and 15 plants per plot. Stars represent the planting location within a given plot.

Data was captured on a subset of the plants in each plot. Within each plot, 3 to 5 plants were randomly selected, while the remaining were cut down and removed. This thinning was done to minimize the overlap between canopies in order to create space to get the Faro scanner in position. It should be noted that the original planting design was used for several other experiments, which required the entire set of plants. In addition, during the data capture process for those other experiments, several of the randomly selected plants sustained damage and had to be removed post LIDAR data collection. The damage included broken branches caused from a wheeled cart being pushed down the rows which changed the biomass and structure of the plant after LIDAR scanning.

Terrestrial laser scanning took place in mid-January 2017. The study used a Faro Focus 3D 120 terrestrial laser scanner. The Focus has a range of 0.6 to 120 m, with a ranging error of ± 2 mm at 10 & 25 m and operates at 905 nm. The scanning was conducted at night to minimize the effect of wind on the pointcloud quality as even a slight breeze can move the foliage, causing noise in the data. The scanning was conducted over a 3-night period and the winds during each night were recorded as negligible, and caused only momentary movement of individual leaves. The scanning took several nights due to the large number of scans and the other data collection which took place in conjunction with this study. The Faro scanner settings were set to a Resolution of 1/5 and a Quality of 3x, with a scanning window of -60° to 90° vertical and 0° to 180° horizontal. This resulted in a scan duration of approximately 2m 39s and a Point Distance of 7.67 mm at 10 m. These settings were chosen as a tradeoff between scan quality and time required to capture data across the entire study. The scanner was mounted on an industrial tripod and was set to a height of approximately 1.25 m. The height varied between scans due to the exact placement of the legs in relation to the local topography. For each plant 2 scans were taken, one from the north and the other from the south side of the plant. The tripod-mounted scanner was placed in the adjacent row (approximately 1.5 m from the center of the target plant) and was aligned so the plant would fall roughly in the middle of the scanning window. In a few cases either an entire plant or some foliage from an adjacent plant was blocking the location for the scanner; in such cases, scans were captured at an angle off of the cardinal direction. No targets were placed in the scene to register the scans; instead the stumps of the removed plants were used along with other objects in the scene. As the scans were completed at night, no color pictures were taken with the scanner. Only the points derived from the laser were used in the analysis.

Field data was harvested starting the day after the first scan. These data included binned biomass data which was binned in 20 cm increments from the soil surface to the top of the plant. The binned data included two separate categories, one for the stalk and stem weights, and a second for the weight of the leaves. The bins were physically marked on each plant, using a large ruler and a number of small pieces of flagging tape to create a set of horizontal planes separating the bins. Prior to harvest, a large tarp was placed around the base of the plant to capture any dropped pieces. Harvesting was done manually by a team of CIAT employees. The harvest was done by first removing all the leaves from a plant and placing them in labelled paper bags for drying. Once all the leaves were removed, the stalks and stems were cut into manageable pieces and again placed in marked bags. The entire harvest took approximately 1 week to complete and another 3 weeks to dry all the samples. To limit molding, a large walk-in cold storage was used to store the samples prior to their time in the dryer. All bags were dried in commercial drying ovens at 70°C and were weighed to capture dry weight.

Data Processing

For the analysis, 54 plants were used. Prior to selecting these plants, the field data was sorted and any plants with missing data were removed from the selection pool. Those plants used for the analysis were randomly selected from the pool by genotype, which resulted in 18 plants per genotype for a grand total of 54 total across the 3 genotypes.

The first step in the analysis was to open each scan file in the Faro SCENE software. This software is required to open the files which are in Faro's proprietary format. For each plant the two scans were registered together in SCENE using common points available in the environment (Figure 8). The target points used were mainly the stalks of the previously removed plants along with some field markers and other objects in the scene. The accuracy of the registration was

assessed through observation of the alignment of objects in the registered pointcloud. Once registration was complete, each plants' pointcloud was roughly clipped to remove unnecessary background points and was then exported as a .xyz file. The .xyz format was chosen to facilitate analysis in other open-source software.

In addition, the unregistered scans (2 per plant) were also roughly clipped and exported as .xyz files to allow single scan analysis. The single scans were used to assess the potential to correlate to the field biomass measures without the need for the registration step. While targets can be used to automate the registration process, this is not always feasible, nor reliable and therefore manual adjustments may still be needed. Thus manual registration, through point picking of common points via various software packages, is often the method used. Our group wanted to assess the potential of bypassing the registration step and using a single scan per plant for the analysis.

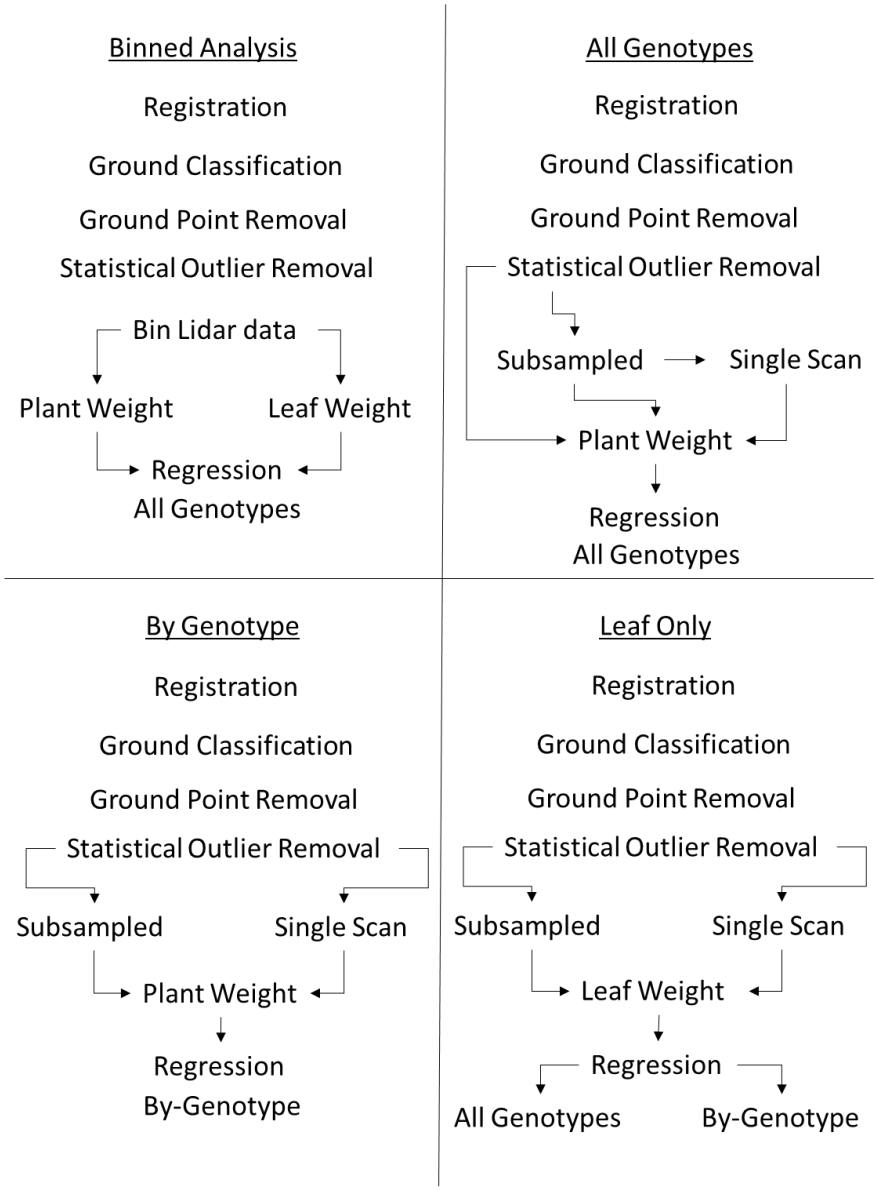

Figure 8. LIDAR data processing and analysis protocol.

The Following processing steps were applied to the registered as well as the single scans. Each pointcloud was opened in Cloud Compare (CC) where it was further clipped to remove all points which were not plant points or ground points which fell below the plant. All the ground points below the plant were kept in order to facilitate the segmentation of ground from plant

points (discussed below). In addition, the Statistical Outlier Filter (SOR Filter) was run to help remove outliers in each pointcloud. The mean distance estimation within the SOR filter was set to 6 points, while the standard deviation multiplier threshold was set to 1.00. These values were determined through trial and error using visual assessment. Each file was then saved in the .las format to allow analysis in R software.

Ground Classification

In R, the lidR package was used to run lasground_pmf (Progressive Morphological Filter) in order to segment the ground points for each pointcloud. The two variables for the filter are: 1) the sequence of window size(s) to be used in filtering the ground returns and 2) the sequence of threshold height(s) above the ground surface to be considered as a ground return (Zhang et al., 2003). For this analysis, trial and error was used to determine the window size of 0.2 m and the threshold height of 0.05 m.

Binning

The next step was to bin the pointcloud data by height to match the field data. The first step was to manually clip the majority of the ground points except for those directly below the main stalk of each plant using CC. These pointclouds were then loaded back into R and the average height of the few remaining ground points was determined. The pointcloud data was binned using the average ground height as a reference and then simply segmenting the data by height to match the field data.

Subsampling

We tested the effect of pointcloud density on the ability of the point count to predict total plant dry weight. To do this the additional preprocessing step of subsampling the pointcloud using the subsampling tool in CC was completed. The minimum space between points was set to

0.002 m (2 mm). This value was chosen as it closely resembles the theoretical maximum ranging accuracy of the Faro Focus 120 (± 0.02 mm @ 10 m) and would not degrade the data.

Data Analysis

All regressions were completed in R using the base lm and all outputs were generated using the package ggplot2. In addition, all bootstrap analyses were conducted using the boot package in R. Bootstrapping is a resampling technique which allows estimation of the population response and associated uncertainty to a variable through sampling with replacement. For details on bootstrapping see Efron & Tibshirani 1994. We used the bias-corrected and accelerated bootstrap (BCa) method as it has the ability to correct for bias and skewness in the distribution of the output estimates. The number of iterations used was 5,000 and the confidence level was set to 0.95. All bootstrap analyses used in this study were conducted using the same method.

To test the ability of the Faro to predict cassava biomass within different height bins we regressed the binned pointcloud data against the binned field data for all 54 plants. The number of points in each pointcloud height bin was regressed against the total dry plant weight (stalk & stem + leaf wts.) and the leaf-only dry weight. A bootstrap analysis was also conducted for both.

Our group examined the relationship between the LIDAR data and the entire plant dry weight. This was done for the registered-only, the registered and subsampled as well as the single scan subsampled LIDAR datasets. For the single scan analysis, the selection of which scan (north or south) to use was done through random selection on a plant-by-plant basis. For each of the three analyses, the point count of each plant's entire pointcloud was regressed against the total plant dry weight. In addition, a bootstrap analysis was also conducted.

Our group also tested the relationship between the LIDAR data and the leaf-only dry weight. This was done for the registered and subsampled as well as the single scan subset

LIDAR datasets. For each of these analyses, the point count of each plant's entire pointcloud was regressed against the total plants leaf dry weight. It should be noted that a few (< 5 %) of the points in each pointcloud were those which hit a stalk or a stem. This value is a liberal estimation of the ratio of stalk & stem to leaf points across the study and is meant to establish the limited effect the stalk & stem points have of the total point count of a given plant. These stalk & stem points were not removed for this analysis as their removal could only be conducted manually, which could potentially cause bias. A bootstrap analysis was conducted for each. A by-genotype analysis using the leaf dry weight was conducted for both the registered and subsampled and the single scan subsampled datasets. This was done by subsetting the dataset by genotype, and then running the same analysis as mentioned above.

The average ratio of leaf to stalk and stem weight for each genotype was determined. This was done by taking the leaf weight for each plant and dividing it by the stalk and stem weight. These ratio values for each plant were then averaged across the genotype. In addition, a shape analysis was conducted to assess the variation in the squareness of the horizontal growth in the X and Y direction for Genotypes 1 and 3. This analysis was done by using the dimensions of the bounding box for each plant in CC. These two dimensions were captured for each plant in the two genotypes and were then turned into a ratio by dividing the two dimensions. The closer the value was to 1.00, the squarer the plant's horizontal growth. A test of equal variance was conducted in R, which found the variances were not equal. A t-test using unequal variances was conducted in R to test if the squareness ratios derived from Genotypes 1 and 3 were equal.

Results

Binned Height

We correlated the binned aboveground biomass data to the binned LIDAR data. Both the total plant dry weight and the leaf-only dry weights were tested. Using the total plant dry weight, we achieved an R^2 of 0.01 with a P-value of 0.02 (data not shown). A slight improvement was seen using only the leaf dry weights, where we found an R^2 of 0.19 at a P-value of 6.62e-9 (Figure 9). The bootstrap analysis suggested an R^2 of 0.19, with a bias of 4.03e-3 and a STDEV of 0.06. The 95 % R^2 confidence intervals for the bootstrap analysis were 0.08 to 0.31.

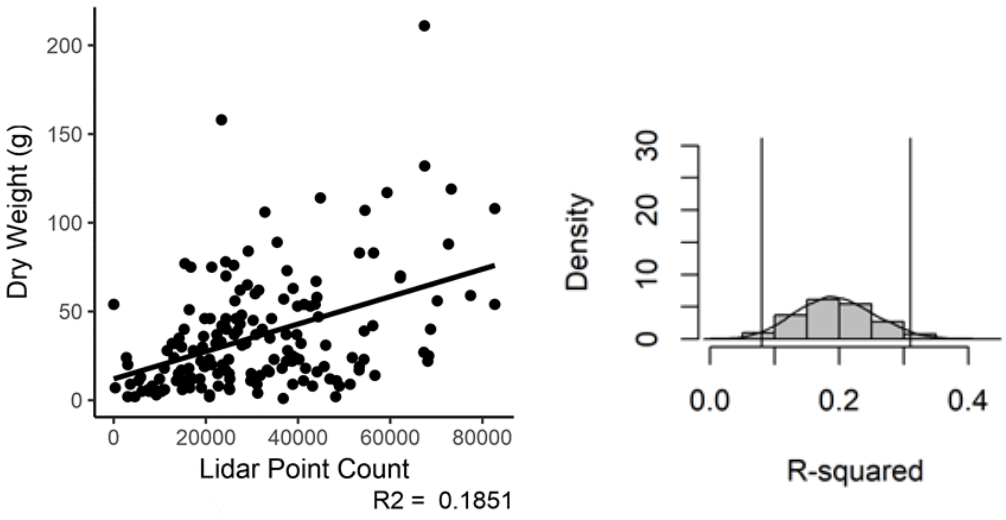

Figure 9. Binned (20 cm) registered and subsampled pointcloud data regressed against the leaf dry weight for all genotypes. Regression (left), bootstrap (right) (n = 349).

All Genotypes Combined

For the registered pointclouds, the total LIDAR point count for each plant was regressed against the entire plant dry weight. The linear regression resulted in an R^2 value of 0.45 and a P-value of 1.73e-08 (data not shown). The bootstrapping resulted in a mean R^2 value of 0.46, a bias of 0.02 and standard error of 0.13. The 95% confidence ranged from 0.21 to 0.7.

To improve the correlation, we took the additional step to subsample each registered pointcloud in an attempt to standardize its spatial density. The subsampling improved the correlation, with an R^2 value of 0.73 and a P^2 of 1.26e-16 (Figure 10). The bootstrap analysis resulted in a mean R^2 of 0.74, a bias of 5.79e-4 and a standard error of 0.07 with a 95% confidence between 0.55 and 0.84.

A major limitation to the use of TLS data, and LIDAR data in general, is the time consuming process of registration. We tested the potential of the point count from a single scan, which was subsampled, to correlate to the entire plant dry weight. The correlation was similar to that obtained via the registered and subsampled clouds. The R^2 value of the regression was 0.73 with a P-value of 2.2e-16 (Figure 11). The bootstrap analysis had a mean R^2 of 0.74, a bias of -8.23e-4 and a STDEV of 0.07. The 95% confidence interval was 0.57 to 0.84.

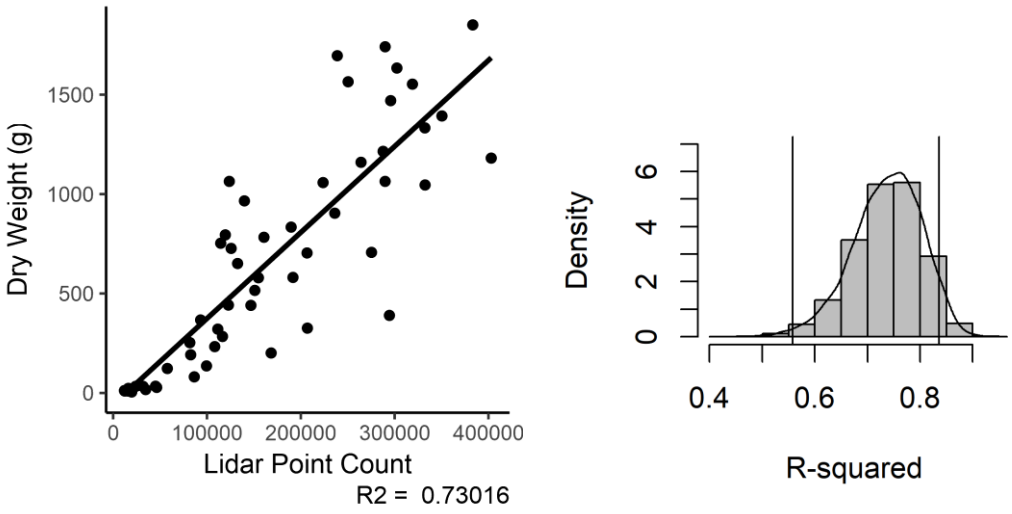

Figure 10. Registered and subsampled pointcloud data regressed against the entire plant dry weight for all genotypes. Regression (left), bootstrap (right) (n = 54).

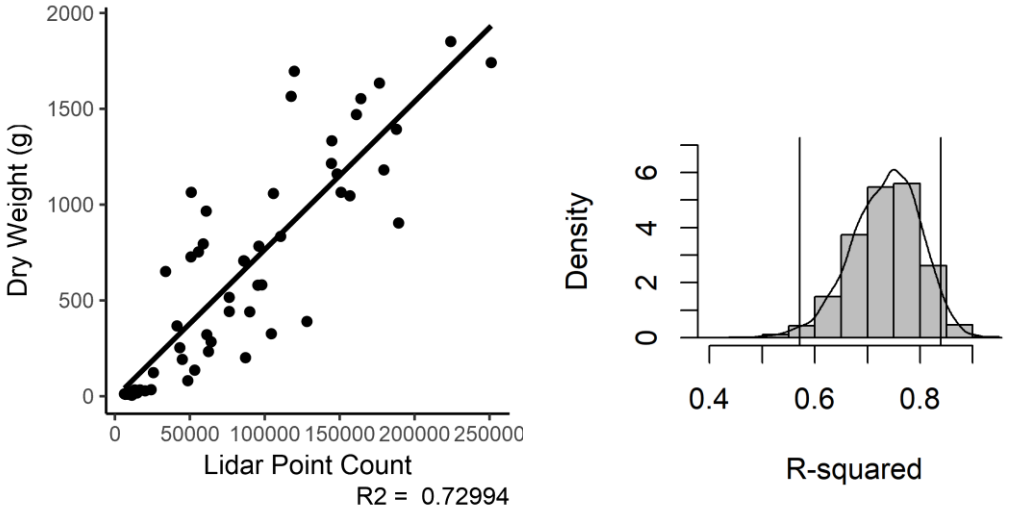

Figure 11. Single scan subsampled pointcloud data regressed against the entire plant dry weight for all genotypes. Regression (left), bootstrap (right) (n = 54).

By Genotype

The study included 3 different genotypes of cassava, which contrasted in their aboveground structure. We tested the ability of the TLS technology to predict plant biomass between the various structural types of cassava. When we assessed the registered and subsampled data on a genotype basis, we found variation in the predictive power of the LIDAR technology (Figure 12). The reader should note that the bootstrap density scale was adjusted to allow full representation of the trend line. Genotype 1 had an R^2 of 0.64 and a P-value of 4.32e-5. Genotype 2 performed well with an R^2 of 0.95 with a P-value of 1.12e-12. Genotype 3 fell in the middle with a R^2 of 0.71 and a P-value of 6.45e-6. The bootstrap results suggest a large amount of variation in the predictive power for both genotypes 1 and 3 (Table 2).

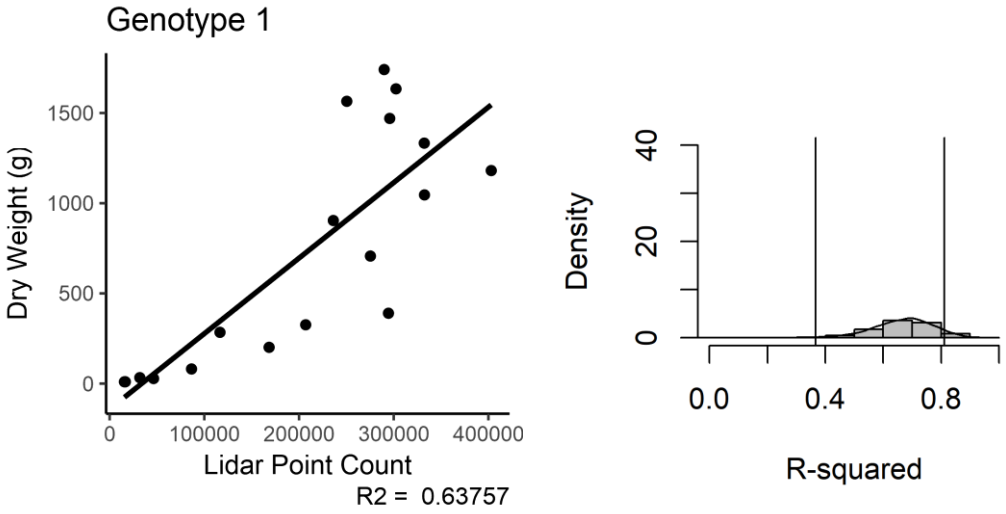

Figure 12. Registered and subsampled pointcloud data regressed against the entire plant dry weight, by genotype. Regression (left), bootstrap (right) (n = 18).

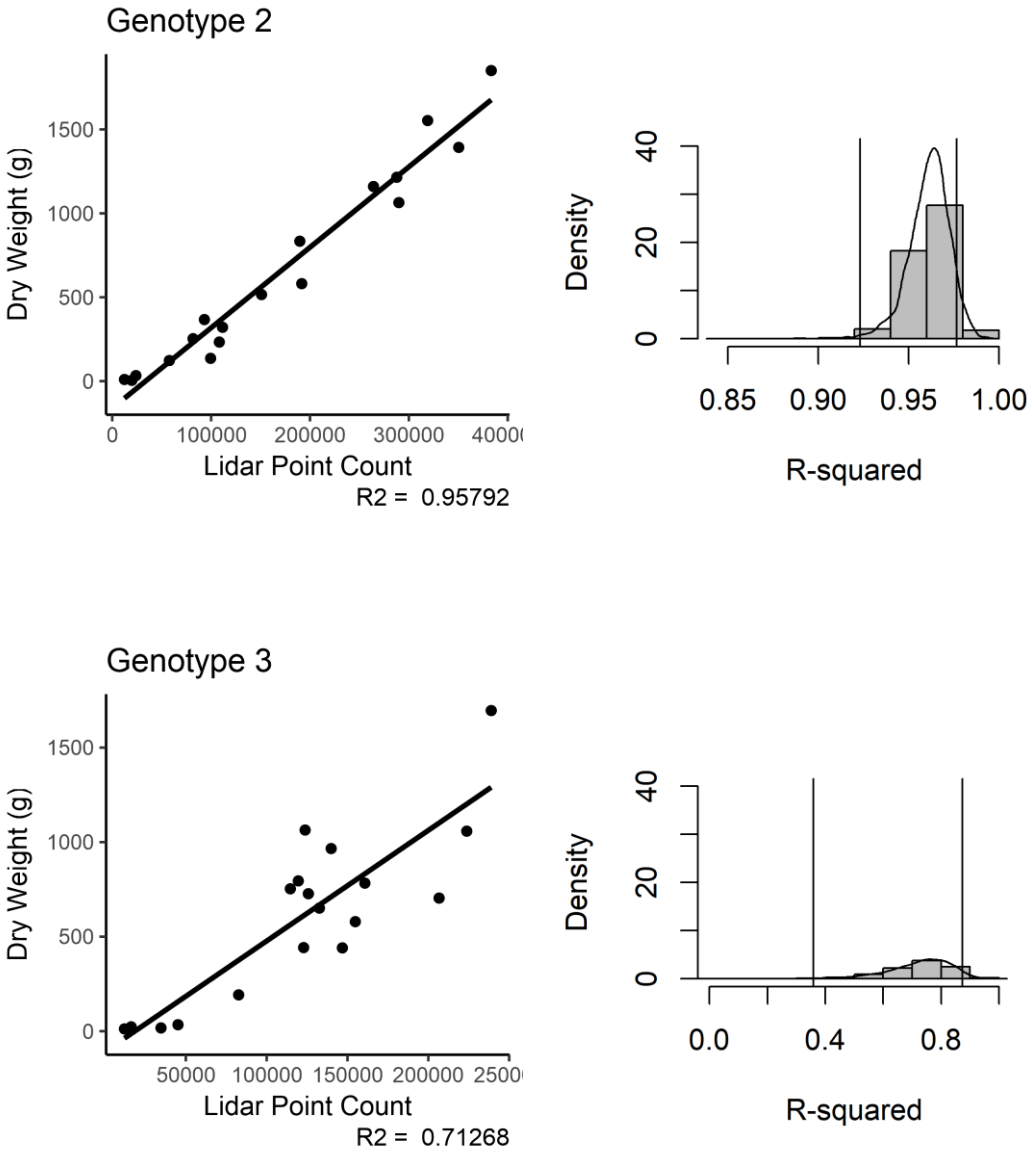

Figure 12. Continued.

Table 2. Registered and subsampled pointcloud data regressed against the entire plant dry weight, by genotype. Bootstrap output (n = 18).

Genotype	Mean R^2	Bias	STDEV	95% Confidence Interval
1	0.66	4.84e-3	0.1	0.36 - 0.81
2	0.96	1.37e-3	0.01	0.92 – 0.98
3	0.73	-7.65e-3	0.12	0.4 – 0.88

The same by-genotype analysis was conducted for the single scan with subsampling dataset. Genotypes 1 and 2 performed similar to the registered and subsampled dataset with specifics in Table 3 in the discussion. However, for Genotype 3, the outcome was not as good. For the 3rd genotype the use of a single scan with subsampling resulted in an R^2 of 0.52 with a P-value of 4.38e-4 (Figure 13). The bootstrap analysis told a similar story, with a notable increase in the range of the 95% confidence interval for Genotype 3 (0.15 - 0.79).

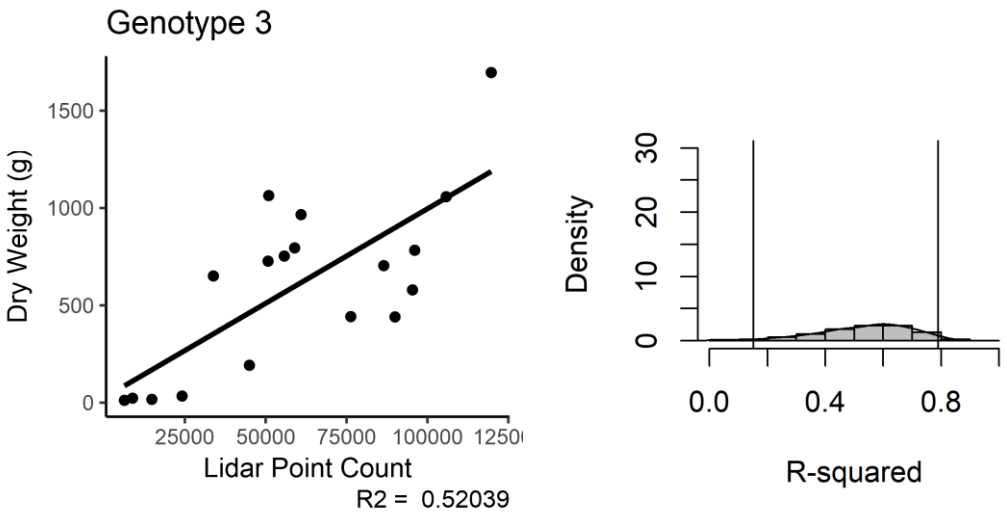

Figure 13. Single scan subsampled pointcloud data regressed against the entire plant dry weight, genotype 3. Regression (left), bootstrap (right) (n = 18).

Leaf Dry Weight

Our group questioned if variations in the stem weights were causing the change in predictive power of the technology between genotypes. In order to test this, we regressed against only the leaf dry weights for both the registered and subsampled and the single scan subsampled datasets.

The first analysis looked at the effect across all genotypes. The registered and subsampled dataset resulted in the best R^2 value of 0.8 with a P-value of 2e-16 (Figure 14). The bootstrap results suggested a 95% confidence interval for the R^2 between 0.63 and 0.88, which again were the best across the study. The single scan subsampled dataset did not perform quite as well with a R^2 of 0.78 (Table 3).

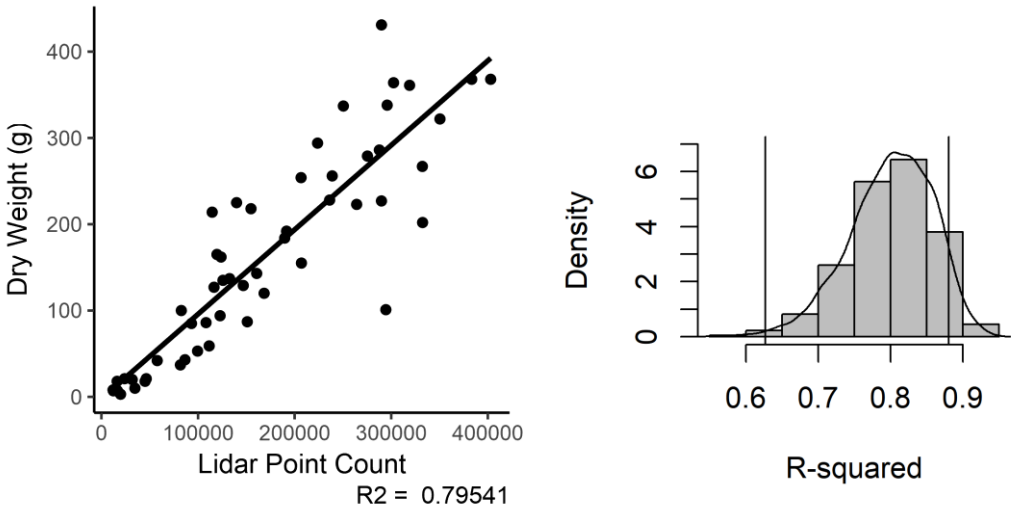

Figure 14. Registered and subsampled pointcloud data regressed against the leaf dry weight for all genotypes. Regression (left), bootstrap (right) (n = 54).

Using the leaf dry weight on a by-genotype basis for the registered and subsampled dataset, resulted in a similar response for Genotypes 1 and 2, as with using the entire plant dry weight (Table 3). However, Genotype 3 had an improved R^2 of 0.83 with a P-value of 1.13e-7 (Figure 15).

We analyzed the single scan subsampled dataset against the leaf dry weights on a by-genotype basis. Interestingly, we found a similar pattern as with the same dataset regressed against the entire plant dry weight. Genotypes 1 & 2 performed about the same (Table 3), while Genotype 3 again performed poorly, albeit with a slight improvement over the entire plant dry weight analysis, with a R^2 of 0.64 and a P-value of 4.31e-5 (Figure 16).

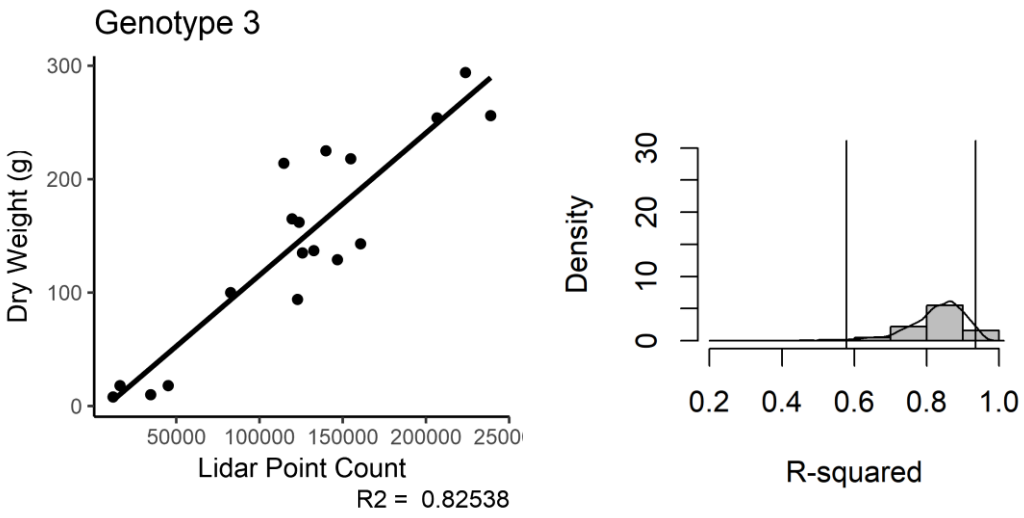

Figure 15. Registered and subsampled pointcloud data regressed against the leaf dry weight, genotype 3. Regression (left), bootstrap (right) (n = 18).

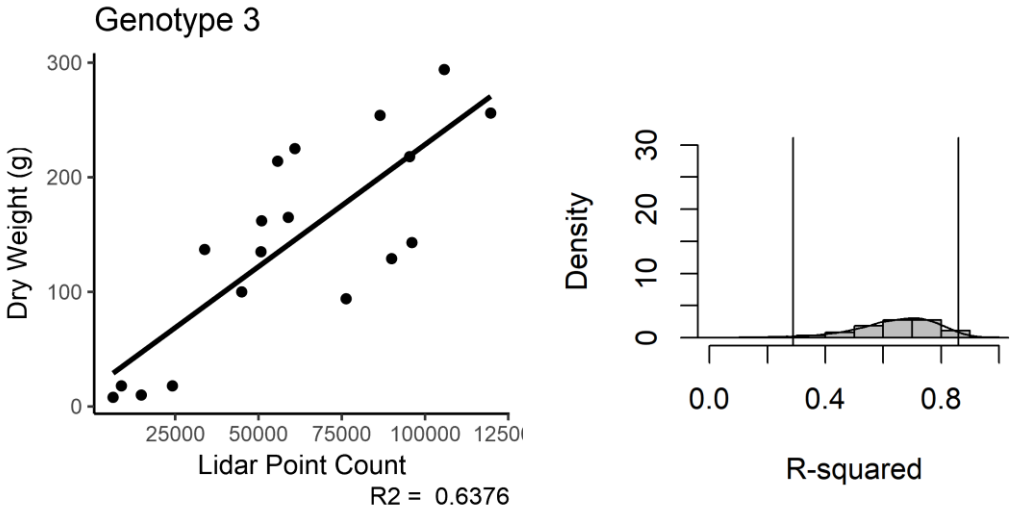

Figure 16. Single scan subsampled pointcloud data regressed against the leaf dry weight, genotype 3. Regression (left), bootstrap (right) (n = 18).

Plant Shape

We compared the ratio of the leaf to stem weights for all three genotypes and found a similar ratio, suggesting variations in the stalk and stem weights may not be a factor in the variation in response between the single scan subsampled methodology and the three genotypes (data not shown). However, when we compared the dimensions of the bounding boxes in CC for each of the plants in Genotype 1 and 3, we found a significant difference (T = -1.77, P-value 0.09) in the ratio of the X to Y axis length (Figure 17). This suggests there is a statistical difference in the shape of the two genotypes.

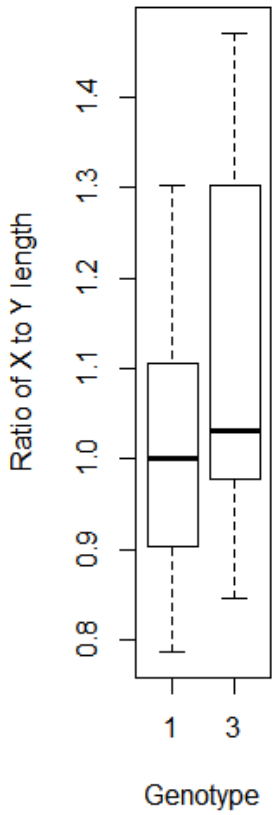

Figure 17. Ratio of the X to Y dimension length by plant for genotypes 1 & 3 (n = 18 per Genotype).

Discussion and Conclusions

The height binned biomass analysis did not work well (R^2 0.01). Using the leaf weight did improve the correlation, though an R^2 of 0.19 is not sufficient to suggest LIDAR as a phenotyping tool for binned height biomass determination. However, several factors could be the cause, and might be addressed in the future. First, the bins may not have overlapped well in respect to the start and end position in the LIDAR data versus the field data. Second, errors related to the placement of the bin start and end locations may have caused noise in the field data. One solution might be to mark the bins on the plant prior to scanning. This would allow more precise overlap to occur between the LIDAR and field data, which might improve the correlation. In addition, this would overcome some of the noise in the field data caused by the imprecise bin locations, further improving the result.

Depending on the processing workflow chosen for the LIDAR data, the strength of the correlation to the entire plant biomass changed. Two key differences existed between the processing workflows: 1) The use of a single scan per plant versus both scans registered together, and 2) and if registered scans were used, whether or not the pointcloud was further subsampled. It should be noted that all single scan analyses included the further subsampling step. The use of the registered only processing methodology resulted in marginal predictability of the entire plant biomass. However, when the same registered dataset was subsampled to produce a uniform point density, the correlation improved (R^2 0.45 to 0.73). Skipping the time consuming and labor intensive step of registration, yet still applying the subsampling, resulted in the same R^2 of 0.73. This result alone suggests there is no need to capture two scans of each cassava plant in order to correlate to the entire plant's biomass, and the registration step can be skipped. This is a major finding, as much of the processing time is spent in the manual registration of scans.

The three genotypes used varied in their aboveground structure. Depending on the processing workflow used (registered and subsampled vs. single scan subsampled) we found the strength of the correlation to the entire plant weight changed, both between genotypes and within. For Genotypes 1 and 2, the use of the single scan subsampled methodology is the best option. However, for Genotype 3 the use of the registered and subsampled method achieved superior results over the single scan subsampled method.

The variation in the response of Genotype 3 between the two analysis methods mentioned previously sparked a comparison between the field derived leaf weight and the LIDAR data. Initial speculation was that structural differences between the genotypes might cause variation in the amount of stalk and stem weight. The stalks, and especially the stems, are hard to capture in the LIDAR data as these parts of the plant are often occluded from view by the leaves. By removing the weight of the stalks and stems, we thought we might improve the overall correlation, as well as improve the response of Genotype 3 to the single scan subsampled analysis method. For Genotypes 1 and 3, using the leaf weight improved the correlation, as compared to regressing against the entire plant weight when the same processing methodology was considered (Table 3). For Genotype 2, the results were good irrespective of the method used, as can be seen in the minimal variation in the statistics between the entire plant and leaf analysis, as well as between the processing methods. However, using the leaf weight with the single scan subsampled method resulted in an improved correlation for Genotype 1, but a lowered one for Genotype 3.

Table 3. Regression and bootstrap results by analysis method using both the dry plant weight and leaf weight for all genotypes (n = 54) and by genotype (n = 18). R = registered; R & S = registered & subsampled; SS & S = single scan subsampled. Grey color denotes R^2 below 0.7.

	Comparing		All Genotypes		
			Regression		Bootstrap
Analysis Method	Plant Weight	Leaf Weight	R^2	P-value	95% CI
R	X		0.45	1.73E-08	0.21 - 0.7
R & S	X		0.73	1.26E-16	0.55 - 0.84
SS & S	X		0.73	2.20E-16	0.57 - 0.84
R & S		X	0.8	2.00E-16	0.63 - 0.88
SS & S		X	0.78	2.00E-16	0.64 - 0.86

	Comparing		Genotype 1			Genotype 2			Genotype 3		
			Regression		Bootstrap	Regression		Bootstrap	Regression		Bootstrap
Analysis Method	Plant Weight	Leaf Weight	R^2	P-value	95% CI	R^2	P-value	95% CI	R^2	P-value	95% CI
R & S	X		0.64	4.32E-05	0.36 - 0.81	0.95	1.12E-12	0.92 - 0.98	0.71	6.45E-06	0.4 - 0.88
SS & S	X		0.73	3.55E-06	0.45 - 0.88	0.96	9.29E-13	0.92 - 0.98	0.52	4.38E-04	0.15 - 0.79
R & S		X	0.7	8.66E-06	0.33 - 0.88	0.95	3.35E-12	0.91 - 0.98	0.83	1.13E-07	0.58 - 0.94
SS & S		X	0.76	1.64E-06	0.45 - 0.91	0.94	3.82E-11	0.89 - 0.97	0.64	4.31E-05	0.3 - 0.86

It is unclear why using the single scan subsampled analysis workflow resulted in a similar, or even superior, correlation in all cases except that of Genotype 3. To try and understand this, we looked at the differences in the horizontal growth shape between Genotypes 1 and 3. We found that Genotype 1 had a more squared growth pattern with less variation between the plants, while Genotype 3 had a more rectangular growth pattern with more variation between plants. An example of this variation can be seen in Figure 18, where an example plant from Genotype 1 has a nearly square bounding box, while the example plant from Genotype 3 has a more rectangular box. The combination of the more rectangular growth pattern along with the greater variation in shape within Genotype 3 may be one cause of the poor performance of the single scan subsampled analysis method for the genotype.

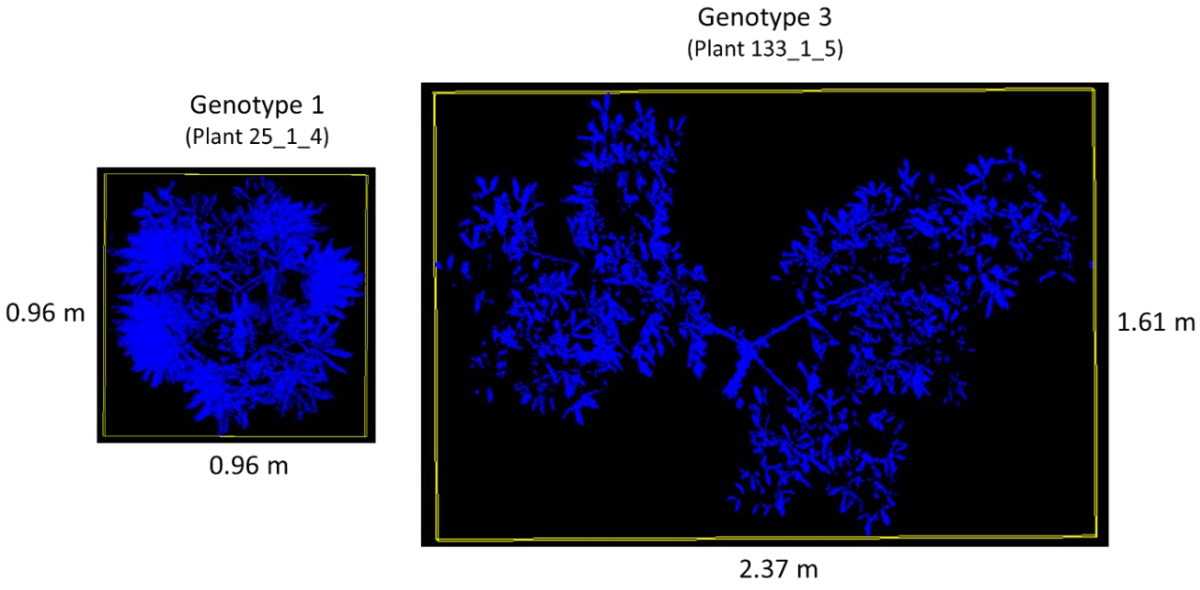

Figure 18. Top down view exported from CloudCompare showing the variation in the shape between Genotype 1 and Genotype 3. Bounding box in yellow.

In our future work, binned field data will be collected using a marker system to allow the alignment of the field bins to those generated in the LIDAR data. Experiments using other crops and cassava genotypes, as well as those using other sensors where a pointcloud is formed, will re-test the use of the single scan subsampled processing workflow and provide a better assessment of the full potential of bypassing the registration step for biomass estimation and phenotyping in general. In addition, there is a significant need to determine what set of factors led to the poor performance of the single scan subsampled processing methodology for Genotype 3. In conclusion, our findings, while positive, suggest there is not a single LIDAR processing workflow which can be applied to all cassava genotypes for the prediction of aboveground biomass. Therefore, we recommend preliminary testing before committing to a processing methodology.

CHAPTER V

A LOW COST 3D PHENOTYPING PLATFORM USING KINECT V2 SENSORS

Introduction

There has been substantial effort to develop high-throughput phenotyping tools within the fields of plant breeding and agriculture (Fiorani & Schurr 2013). Many of these traditional phenotyping tools utilize 2D images captured from satellites or planes, while more recently the benefits of 3D analysis techniques have become apparent. Three-dimensional analysis tools allow the characterization of factors such as plant architecture to play a major role in the remote phenotyping process. However, high precision 3D phenotyping tools, such as airborne and terrestrial laser scanners and flash LIDAR, are often not practical as their purchase costs are often in excess of a $100,000 USD. Despite their prohibitive cost, a large body of research exists on the use of 3D imaging tools within the biological sciences (Popescu 2007; Eitel et al., 2014; Ma et al., 2016). Phenotyping with 3D data has proven successful, with many studies showing significant correlation to biomass (Ehlert et al., 2010), plant height (Tilly et al., 2014), and other phenotypic traits (Hosoi et al., 2011). However, two broad issues still limit the widespread use of many 3D plant phenotyping platforms: 1) The complexity of the data analysis process and 2) the substantial platform acquisition costs. Here we make an attempt to eliminate the cost barrier through the utilization of consumer-grade depth cameras, off the shelf parts, and custom software which will be provided open-source.

While commercial laser scanners have seen quality improvements with reduced costs, they are still far out of reach for all but the largest organizations. However, demand for 3D data in the development of autonomous vehicles and interactive gaming (Naranjo-Hernández et al.,

2017) has led to the production of low-cost sensors known broadly as “depth sensors.” These sensors generally utilize one of three principles to create this depth data: stereo vision, structured light, or time-of-flight (Islam et al., 2017). But with their low cost comes limitations, such as a reduction in accuracy and precision as well as a lack of stability across operating environments. In particular, depth sensors which utilize active sensors are often affected by strong light, and thus are not well suited for outdoor daytime use. While this is generally not an issue for stereo vision sensors, they often perform poorly when used in complex environments, such as agriculture fields, which lack the pronounced features required for depth estimation (Rosell-polo et al., 2017). Despite these limitations, depth sensors have been explored as tools to produce 3D data within agriculture and related fields. In particular, the two RGB-D sensors (an RGB camera and depth sensor combined) produced by Microsoft for use with their gaming consoles have been used extensively by the research community. The Kinect Version 1 (released 2010) and Version 2 (released 2014) both proved to be unpopular within the video game industry (Wilson 2017), but nevertheless have found life as a low cost, lightweight alternative to terrestrial laser scanners in the fields of computer vision (Han et al., 2013), medicine (Galna et al., 2014) and ecology (Azzari et al., 2013).

The Kinect V2 sensor was released in July 2014 and included several improvements over its predecessor. Arguably, the most significant change was the use of an infrared (IR) time-of-flight sensor over the structured light sensor found in V1. This change resulted in a reduction of noise, improved depth accuracy, and a higher framerate (Zennaro et al., 2015). Additionally, the RGB camera used in the Kinect V2 is of a higher quality than that found in the older version. However, as a low cost sensor the Kinect V2 has some limitations related to depth image accuracy, noise from ambient light (Lachat et al., 2015$_b$), and sensor-to-sensor interference

(Kunz & Brogli 2016). Extensive research has been conducted on the performance and limitations of both versions of the Kinect sensor (Otte et al., 2016). The low cost lens used on the V2 sensor has inherent flaws, which cause errors in the depth measurements that worsen radially from the center of the depth image. These errors can be several centimeters at the extreme corners of the depth image when captured at distances over 3 m (maximum range is 4.5 m). However, a distance error no greater than ± 5 mm throughout the effective range of the sensor can be expected as long as the data in the far corners of the image are not considered. While not as susceptible as the Kinect V1, direct sunlight, especially when cast on the sensor itself, will cause distortions ranging from noise to total loss of data. However, this can be largely overcome under field conditions by collecting data during periods of low light or at night. Since every Kinect V2 sensor uses the same IR light source, interference between multiple sensors is possible. This could be avoided if the modulation frequency could be adjusted, but this is not an option available to the user. Therefore, the field of view of multiple sensors should be such as to minimize interference during the random periods when the IR diodes are in sink (Kowalski et al., 2015). Another option to overcome this is to trigger the sensors manually in sequence; however, this solution might not be valid if the object of interest is in motion.

Methods

In an attempt to combat the high cost of entry into the fields of 3D phenotyping and crop analysis, we combined low cost and readily available parts to produce a field-ready 3D imaging tool (Figure 19). Our current version of the platform is named “Scorpion” based on the shape of the frame, which holds the depth sensors. Our platform consists of: Microsoft Kinect V2 sensors, LattePanda™ brand single board computers (SBC), a router, smartphone, and a battery with a power inverter. The only parts of the platform which are not consumer products are 1) the

software, which activates the sensors and stores the data, 2) the frames, which grasp each sensor under compression, and 3) the structure, which holds all of the sensors in place. A detailed parts list with associated costs can be seen in Table 4.

Figure 19. A low cost 3D imaging platform named Scorpion.

Table 4. Detailed Scorpion parts list with itemized costs. *Item count is in parenthesis if greater than 1. **Cost is an estimate of manufacture by a custom fabrication shop.

Part	Cost (USD)
Microsoft Kinect V2 (3)*	$450
Microsoft Kinect V2 Windows PC wiring adapter (3)	$150
LattePanda 4g/64g single board computer (3)	$450
Wagan Elite 400 w Pure Sine Wave inverter	$140
Smart Battery 12 V 50 Ah Lithium Ion battery	$700
Surge protector	$20
USB power brick	$20
Basic home router	$30
Custom Aluminum case for LattePanda boards*	$100
68 L plastic storage tote	$20
50mm USB fans (5)	$30
Custom Aluminum frame for Kinects (3)* **	$200
Square tube structure to hold sensors**	$250
Total	$2,560

The platform uses three Microsoft Kinect V2 sensors, although future platforms could be built to hold any number of sensors. The sensors were purchased for $150 USD and the proprietary wiring required to connect the sensor to a computer was an additional $50 USD. The manufacturer's specifications for the sensor are listed in Table 5.

Table 5. Listed specifications of the Microsoft Kinect V2.

Feature	Value
Color Camera	1920 x 1080 @ 30fps
Depth Camera	512 x 424 @ 16 bits
Min Depth Distance	50 cm
Max Depth Distance	450 cm
Horizontal FOV	70 degrees
Vertical FOV	60 degrees
USB	3.0
Supported Operating System	Win 8 or newer

Each Kinect sensor utilizes nearly the entire bandwidth of a USB 3.0 bus; therefore, a dedicated bus is required for each sensor. Additionally, the Kinect SDK 2.0 used to operate the sensor requires Windows 8.0 or higher. Our solution to meet these conditions was to use a Windows-enabled SBC with USB 3.0 capability. We chose the 4g/64g model of the Windows 10 enabled SBC from the manufacturer LattePanda. For details see Figure 20 & Table 6.

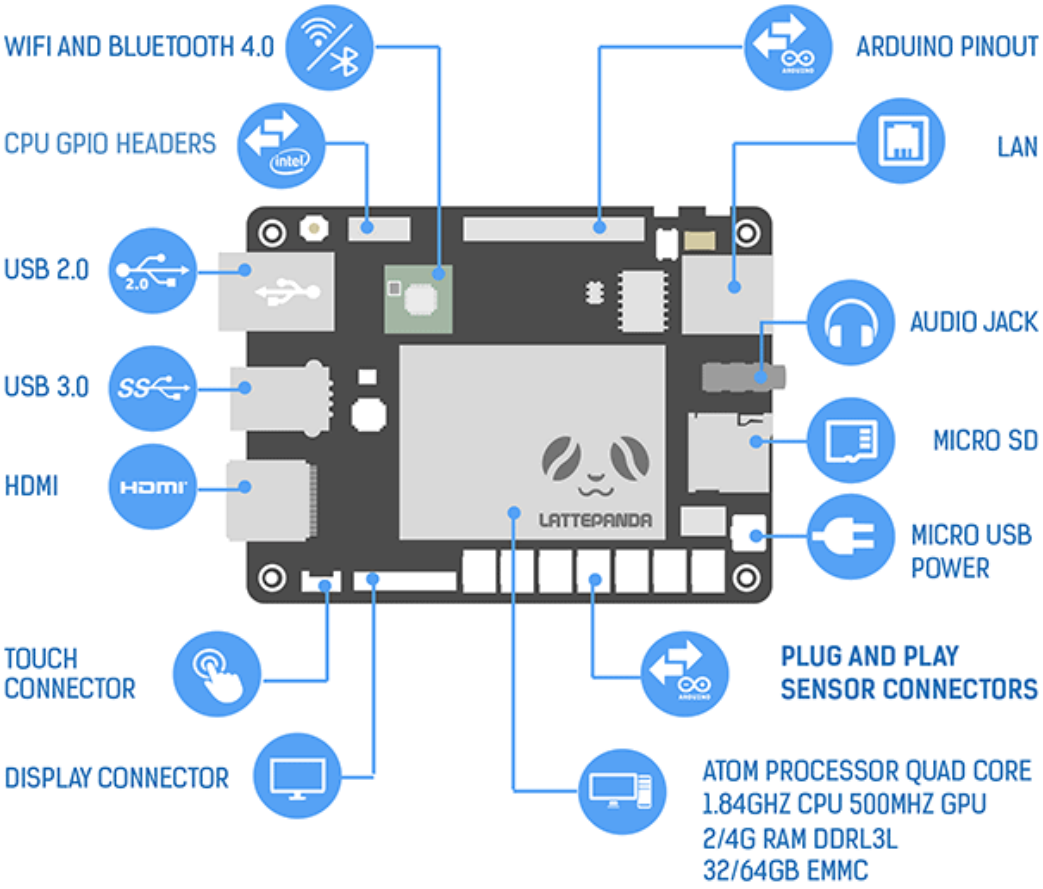

Figure 20. Features of the LattePanda 4g/64g single board computer. Image curtesy of lattepanda.com, 2019.

Table 6. Specifications of the LattePanda 4g/64g model.

Feature	Value
Processor	Intel Cherry Trail Z8300 Quad Core 1.8GHz
Operating System	Windows 10
Ram	4 GB DDR3L
Storage	64 GB
GPU	Intel HD Graphics, 12 EUs @ 200-500 Mhz, single-channel memory
USB ports	1-USB 3.0 & 2-USB 2.0
Wireless Communication	WiFi & Bluetooth 4.0
Arduino	ATmega32u4
Video out	HDMI & MIPI-DSI
Power	5V/2A
Dimensions	88 x 70 mm

For our setup, one SBC was required for each Kinect V2 sensor (Figure 21). This is because each SBC only has one USB 3.0 bus. Each SBC was set to boot upon receiving power. An aluminum case was constructed to hold the three SBCs, which included two 50 cm USB-powered fans with filters to minimize dust and cool the computers. Each Kinect sensor and SBC was plugged into a 6-slot surge protector for power. The surge protector was subsequently plugged into a 400 W pure sine wave inverter by Wagan Tech ™. The inverter received its power from a 12 V 50 Ah Lithium Ion battery from Smart Battery ®. While expensive, this

battery was lightweight and allows for a total discharge, unlike lead acid or AGM types. An additional USB power strip was plugged into the inverter's USB power port to power all the fans. The last outlet plug on the inverter was used to power a wireless router, which allowed communication between the SBCs and the smartphone. All of these parts were placed inside of a roughly 68 L plastic storage tote for hand transport through the field. In order to keep the parts cool, three holes were drilled and fitted with additional 50 mm fans and filters, which circulated air through the box. A final 2.54cm hole was drilled to allow the cords of each Kinect sensor to pass though.

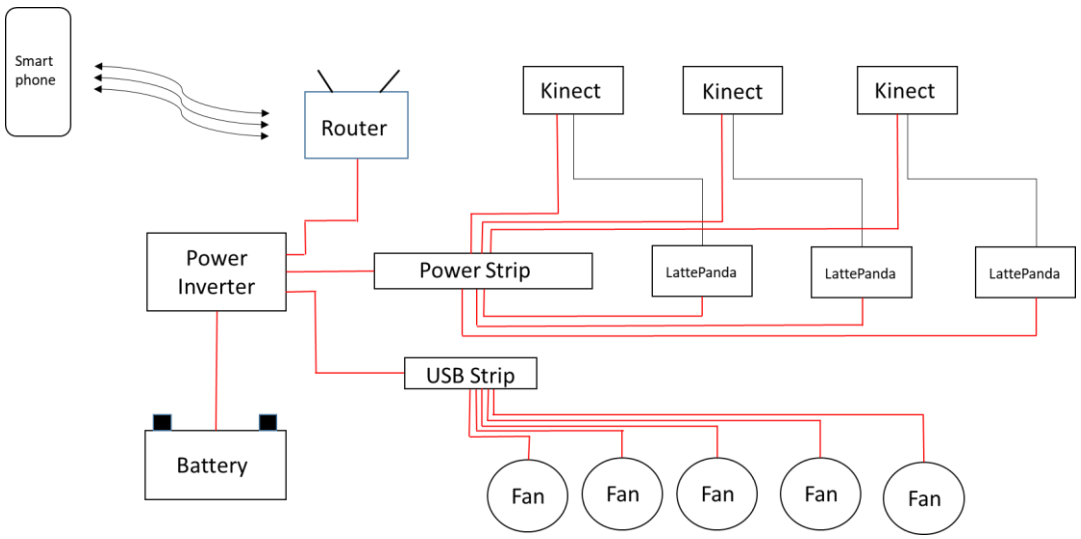

Figure 21. Kinect platform hardware.

Three Kinect sensors were used in this version of the platform. While more sensors could be used, the weight of the larger structure and additional sensors would limit its portability. The structure was made out of 3 cm steel square tubing with a 1.98 mm wall thickness. The structure

consisted of 2 parts: a base and top. The base is an H design so that the structure is stable on uneven terrain. The top portion was designed to position the sensors at slightly different viewpoints while minimizing the overall footprint and maintaining balance. The base was attached to the top portion via a single bolt verses a welded joint to minimize any tension in the structure and allow height adjustment. Each Kinect V2 sensor was attached to the structure by a custom-made frame. The frame was made out of aluminum to reduce weight and used a combination of compression and friction to hold the sensor. Rubber strips were glued on the top inside of the frame and bolts with aluminum backed 2.54 cm diameter rubber disks were used to sandwich the sensor in place. While this system is not the most robust, it fared well and required no modification to the Kinect sensor. The frame was bolted onto the structure and tightened to hold the sensor at the desired angle. Blue Loctite (Henkel AG & Company, KGaA), a thread locking chemical, was used to insure the connections did not come loose.

To operate the platform a custom-made open source application was created. The Scorpion app is a web application that utilizes the communication layer of the Microsoft RoomAlive toolkit (Jones et al., 2014) to allow the Kinect sensors, LattePanda boards and the user to carry out acquisition of 3D data (unpublished). The application was built in C# using the Kinect SDK 2.0, while the graphical user interface (GUI) was developed entirely in ReactJS. With this app the user is able to remotely control the entire platform by utilizing interface features to turn on the system, capture an image (create the pointcloud), visualize and store the data and restart or power off the system (Figure 22). The Scorpion app allows an unlimited number of sensors to be networked together, provided that they, along with the user access device (cell phone, tablet, etc.), are connected to the same Wi-Fi SSID.

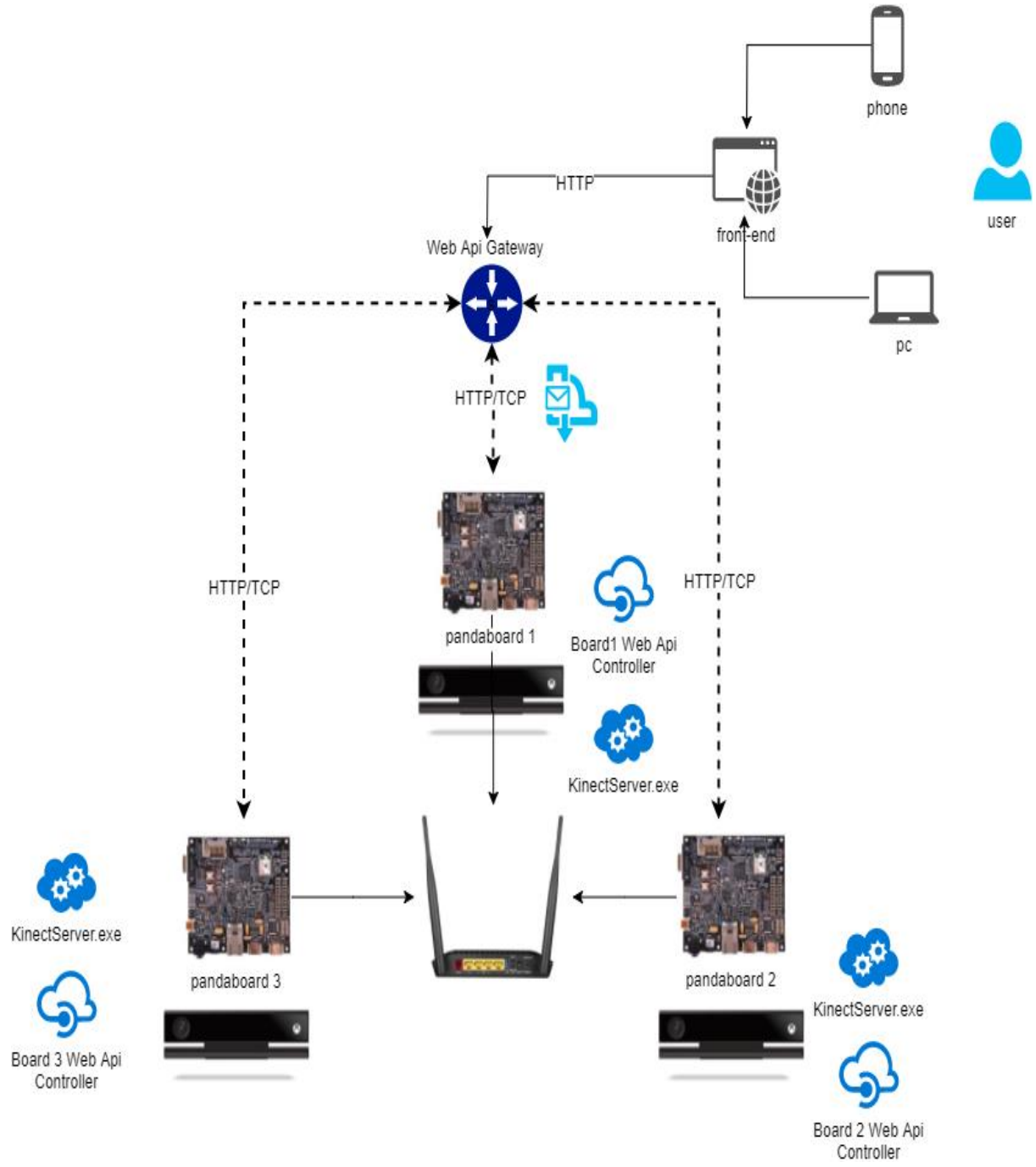

Figure 22. Scorpion app communication.

The user is able to access the Scorpion app from any device that is connected to the same Wi-Fi network as the SBC's. Each SBC will run Windows 10, along with these three applications:

1) Scorpion Web Application.
2) Web API Gateway: An API REST built in C# which processes the requests that the user makes from the interface. The API is responsible for sending the order to the corresponding sensor via a socket.
3) KinectServer.exe: This application was built using WCF (Windows Communication Foundation). The 2.0 version of the Kinect SDK works as an Interface (endpoint) between each sensor connected to the scorpion and the Web API gateway.

Figure 23 outlines the components of the scorpion web controller application separated into the presentation and business tiers.

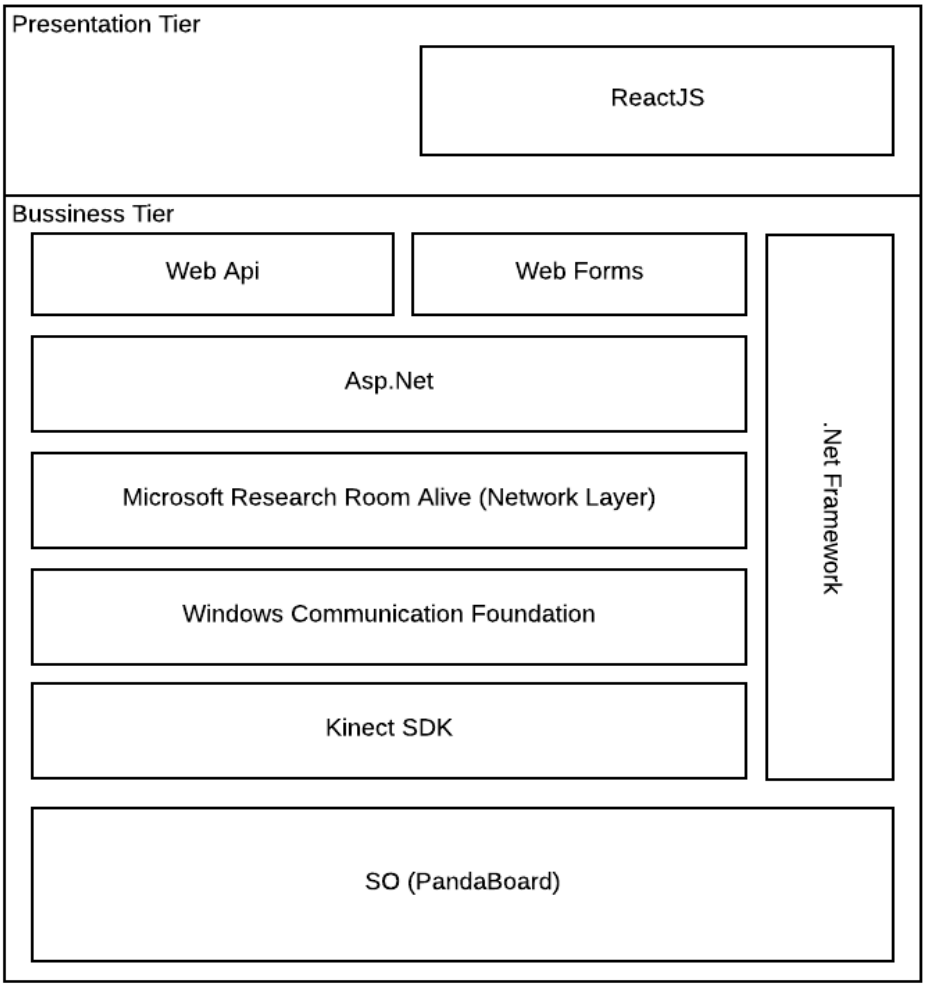

Figure 23. Accessing the Scorpion web controller app.

Field Operations

Prior to any data collection campaign, the desired camera poses and distance from the object to the structure should be determined based on the sample. Consideration should be given to the fact that the further from the object the structure is placed, the sparser the dataset will be for any one area of interest. Additionally, some overlap of the field of view of each sensor is needed to allow manual target-based registration. Once each sensor position is set, the pose of

each needs to be determined so that the three depth images can be registered to form a single pointcloud. This can be done by capturing a set of depth images of a static scene which has recognizable items for point-to-point registration. When performing the registration, select the camera which captures the middle of the scene as the reference and register the other two cameras to it. The two transformation matrices, one for each camera that were transposed, should be copied. Each matrix is then applied to each image captured from the same camera in order to rapidly register the rest of the depth images. If multiple data capture positions will be used around a single object, then static targets will need to be placed or occur naturally in the data to allow registration.

Due to the issue of sensor-to-sensor interference, each Kinect will be triggered in sequence. Therefore, any motion of the object(s) in the scene will be captured, possibly resulting in poor performance. If this platform is used in an agriculture field setting, we recommend collection of data when there is as little wind as possible. To combat the issue of light sensitivity, we recommend that data be captured at night. This will also help with the problem of motion, as generally the early hours of the morning are the most calm.

Two people are required to operate the Scorpion: One person to position the structure and another to move the tote. Any smartphone or tablet on the local Wi-Fi network can be used to access the web application in order to trigger the data collection sequence. Along with data collection, the web application can be used to view the files, delete existing files, and assign the naming convention. The 50 Ah battery under normal field conditions will last in excess of 4 hours. With Windows 10 home edition and the Scorpion software installed, approximately 20 GB of space is available for data storage on each SBC. This should allow at least 2000 samples to be captured, though an external drive could be added to the system to expand capacity. The

time required to align the structure with the object of interest and capture data using the three sensors was approximately 15 seconds. Once the campaign is complete, an external drive can be connected to the main LattePanda or a local area connection can be made to extract the data.

Preliminary Campaign

Throughout the development of the Scorpion, tests were conducted to help insure a viable platform would emerge. We conducted a laboratory comparison of the data produced from a Kinect V2 and that from a Faro Focus 120 (unpublished). We also conducted tests to better understand the effect that varying sunlight intensity had on the Kinect data quality (unpublished). However, without traditional field tests, uncertainty would exist as to the performance of the platform for 3D plant phenotyping. This structure of the Scorpion was designed to sample cassava (*Manihot esculenta*) at the International Center for Tropical Agriculture (CIAT) in Cali, Colombia, though we had no access to the cassava for our preliminary tests. Ragweed (*Ambrosia psilostachya*) is common in the area around Texas A&M University and has a similar leaf architecture to cassava. Therefore, we decided to use ragweed as a proxy to test the Scorpion.

Four bunches of ragweed with similar biomass were sampled. The bunches were marked out in the daylight to insure general uniformity and ease of access. Prior to going to the field, several depth images were captured indoors to provide the transformation matrix. Each bunch was sampled one time from a distance of approximately 1.5 m from the southern side. The next morning, each bunch was harvested and then dried in a dryer for approximately one week until each bag's weight held constant for a 24-hour period.

The data collected with the Scorpion was copied onto a Dell workstation laptop for analysis which was conducted with the open source software CloudCompare. The first step was to register the indoor depth images to determine the transformation matrices. The camera

positioned in the middle of the scene was used as the reference and the other two cameras were registered to it. This created two transformation matrices, one for each of the two remaining cameras. These same matrices were then applied to each depth image derived from the assigned camera. For specific instruction on how to register scans and capture the transformation matrix, see the CC help files.

Once the depth images from each of the three sensors were registered into a single pointcloud, further processing was conducted in CloudCompare. All the points around each bunch were manually clipped to leave only the data which represented the ragweed. Next, the Statistical Outlier Filter (SOR) tool was used to remove the majority of the noise from each of the pointclouds. The settings used for the SOR were chosen based on a visual assessment of the quality of the resultant pointcloud. The last step taken was to thin each dataset to help normalize the point density. This was done with the subsampling tool, where a space-based thinning approach was used. Finally, the point count of each pointcloud was recorded and a regression analysis was conducted against the ragweed dry weights, where an R^2 of 0.89 with a P-value of 0.04 was found (Figure 24).

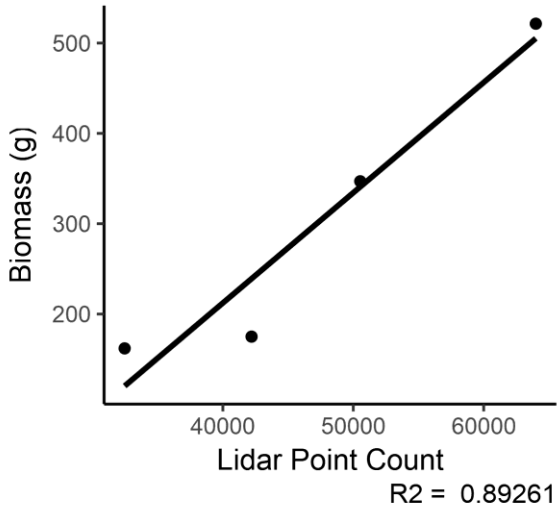

Figure 24. Regression analysis of point count versus dry ragweed biomass.

Discussion and Conclusions

While the results of the preliminary analysis were welcomed, caution must be used as the sample size (n = 4) was very low. However, the low sample size was thought sufficient for this preliminary analysis, as the main goal was to test platform functionality related to field performance and software stability. In this regard the platform performed well. The structure, while heavy, was stable even on top of dense grass. The software is generally stable, though the software has a function to restart the Kinect server script, if any malfunctions occur.

The next step is to capture data on cassava with both the Scorpion platform and a high-end terrestrial laser scanner, the Trimble TX5. A comparison between the quality of the pointclouds captured, along with the regressions produced against the dried biomass, with these two 3D imaging platforms will be made. Our long-term objective is to automate the collection of data with the Kinect sensors by mounting them on an autonomous vehicle, which can sample

during ideal periods of low wind and light. This vehicle will use RTK-corrected GPS locations to navigate through the field and capture data in the correct positions. It will also gather wind and light data, which will be used to trigger data capture only under ideal conditions.

CHAPTER VI

CONCLUSIONS

There is a major phenotyping bottleneck limiting the development of the elite cultivars required to provide food security in the coming decades. The work here is a small, but significant step towards overcoming this bottleneck. Cassava is a global crop utilized mainly by subsistence farmers for its starch-rich roots, ample aboveground forage and ability to thrive on marginal soils. Considering the global importance of cassava, it has seen only marginal breed improvements and little investment in high-throughput phenotyping techniques.

We took a first step towards this investment by testing the terrestrial laser scanner as a tool for rapid estimation of cassava height under field conditions. We studied 3 different genotypes, which varied in their aboveground structure, and were able to predict their combined height with a high degree of accuracy ($R^2 = 0.81$). However, manual corrections of the individual plant segmentations produced by the tree classification algorithm used were required. Overlap in the canopy, especially for genotype 3, caused error in the classification, leading to poor height estimation. This was made clear when the genotypes were assessed independently, as Genotypes 1 and 2 had improved correlations from the combined analysis with a R^2 of 0.88 and 0.9, respectively. Placement of the scanner in an elevated position and increasing the number of scan positions, especially when assessing genotypes with overlapping canopies, might help to increase the predictive power of the technology. In addition, other segmentation algorithms might work better with overlapping canopies and should be investigated.

Aboveground biomass is another common phenotypic trait used for development of improved cultivars and is an important trait in the breeding of cassava. Since the terrestrial laser

scanner proved well suited for the prediction of cassava height, we took the next step of using the technology to estimate biomass. We again used 3 genotypes, which contrasted in their aboveground structure, to test the ability of the technology to predict the aboveground total plant biomass as well as the leaf biomass in cassava. We found that the scanning methodology and the processing workflow both had a major impact on the predictive power. Our study concluded that the use of a single scan per plant was generally adequate, thus saving time both in the field and through the removal of the registration step during the analysis. However, depending on the genotype being assessed and the level of accuracy required, our results suggest the use of 2 scans can add marginal improvement to the predictive power. In addition, we found that subsampling of the pointcloud greatly improved the correlations across all genotypes, which is possibly an artifact of the smoothing of the point density from the front to the back of the scan. We suspect the varying strength of the correlations between genotypes is related to the overall plant structure and its effect on the laser lights' ability to penetrate the canopy and produce a representative model. Further work needs to be completed to determine the cause of this variable response.

The cost of data acquisition using the terrestrial laser scanners mentioned in this study were high. Much of these costs came from the scanner rental, which were several thousand dollars (USD) per week. The cost of most LIDAR units, especially when mounted to an airborne platform, is a significant barrier to the advancement of the technology for use in high-throughput phenotyping. Nonetheless, other technologies can be used to capture 3D data, for a much more attractive purchase price. However, none of these alternative technologies are an exact replacement for LIDAR, and thus have some significant limitations, generally related to limited range and environmental pitfalls. As an attempt to overcome the cost barrier and increase the interest in 3D phenotyping, we developed a low-cost and field-worthy 3D high-throughput

phenotyping platform. We used off the shelf parts along with custom-made software to produce a phenotyping platform designed around the Microsoft Kinect V2 sensor. We demonstrated that for around $2,500 (USD), and working around a few limitations related to direct sunlight and sensor-to-sensor interference, a field-worthy platform can be built. Our future work will compare the accuracy of a traditional terrestrial laser scanner to that of our Kinect-based platform, both in a laboratory and under field conditions.

REFERENCES

Alenyà, G., Dellen, B., Foix, S., & Torras, C. (2013). Robotized plant probing: Leaf segmentation utilizing time-of-flight data. *IEEE Robotics & Automation Magazine*, *20*(3), 50-59.

Andersen, M. R., Jensen, T., Lisouski, P., Mortensen, A. K., Hansen, M. K., Gregersen, T., & Ahrendt, P. (2012). Kinect depth sensor evaluation for computer vision applications. *Aarhus University*, 1-37.

Andújar, D., Dorado, J., Fernández-Quintanilla, C., & Ribeiro, A. (2016). An approach to the use of depth cameras for weed volume estimation. *Sensors*, *16*(7), 972.

Anthony, D., Elbaum, S., Lorenz, A., & Detweiler, C. (2014). On crop height estimation with UAVs. In *2014 IEEE/RSJ International Conference on Intelligent Robots and Systems* (pp. 4805-4812). IEEE.

Araus, J. L., & Cairns, J. E. (2014). Field high-throughput phenotyping: the new crop breeding frontier. *Trends in plant science*, *19*(1), 52-61.

Arnó, J., Vallès, J. M., Llorens, J., Sanz, R., Masip, J., Palacín, J., & Rosell-Polo, J. R. (2013). Leaf area index estimation in vineyards using a ground-based LiDAR scanner. *Precision agriculture*, *14*(3), 290-306.

Azzari, G., Goulden, M., & Rusu, R. (2013). Rapid characterization of vegetation structure with a Microsoft Kinect sensor. *Sensors*, *13*(2), 2384-2398.

Buckley, S. J., Howell, J. A., Enge, H. D., & Kurz, T. H. (2008). Terrestrial laser scanning in geology: data acquisition, processing and accuracy considerations. *Journal of the Geological Society*, *165*(3), 625-638.

Busemeyer, L., Mentrup, D., Möller, K., Wunder, E., Alheit, K., Hahn, V., ... & Rahe, F. (2013). BreedVision—A multi-sensor platform for non-destructive field-based phenotyping in plant breeding. *Sensors*, *13*(3), 2830-2847.

Butkiewicz, T. (2014). Low-cost coastal mapping using Kinect v2 time-of-flight cameras. In *2014 Oceans-St. John's* (pp. 1-9). IEEE.

Byrne, D. H., Guerrero, J. M., Bellotti, A. C., & Gracen, V. E. (1982). Yield and plant growth responses of Mononychellus mite resistant and susceptible cassava cultivars under protected vs. infested conditions. *Crop Science*, *22*(3), 486-490.

Cabrera-Bosquet, L., Crossa, J., von Zitzewitz, J., Serret, M. D., & Luis Araus, J. (2012). High-throughput Phenotyping and Genomic Selection: The Frontiers of Crop Breeding Converge F. *Journal of integrative plant biology*, *54*(5), 312-320.

Cabrera-Bosquet, L., Molero, G., Stellacci, A., Bort, J., Nogues, S., & Araus, J. (2011). NDVI as a potential tool for predicting biomass, plant nitrogen content and growth in wheat genotypes subjected to different water and nitrogen conditions. *Cereal Research Communications*, *39*(1), 147-159.

Ceballos, H., Okogbenin, E., Pérez, J. C., López-Valle, L. A. B., & Debouck, D. (2010). Cassava. In *Root and tuber crops* (pp. 53-96). Springer, New York, NY.

Ceballos, H., Iglesias, C. A., Pérez, J. C., & Dixon, A. G. (2004). Cassava breeding: opportunities and challenges. *Plant molecular biology*, *56*(4), 503-516.

Chang, S., Zhao, L., Timilsina, G. R., & Zhang, X. (2012). Biofuels development in China: Technology options and policies needed to meet the 2020 target. *Energy Policy*, *51*, 64-79.

Chen, C., Jafari, R., & Kehtarnavaz, N. (2015). Utd-mhad: A multimodal dataset for human action recognition utilizing a depth camera and a wearable inertial sensor. In *2015 IEEE International conference on image processing (ICIP)* (pp. 168-172). IEEE.

Chéné, Y., Rousseau, D., Lucidarme, P., Bertheloot, J., Caffier, V., Morel, P., ... & Chapeau-Blondeau, F. (2012). On the use of depth camera for 3D phenotyping of entire plants. *Computers and Electronics in Agriculture*, *82*, 122-127.

CloudCompare (version 2.8.1) [GPL software]. (2018). Retrieved from http://www.cloudcompare.org/

Connor, D. J., & Cock, J. H. (1981). Response of cassava to water shortage II. Canopy dynamics. *Field Crops Research*, *4*, 285-296.

Corti, A., Giancola, S., Mainetti, G., & Sala, R. (2016). A metrological characterization of the Kinect V2 time-of-flight camera. *Robotics and Autonomous Systems*, *75*, 584-594.

Davis, J. P., Supatcharee, N., Khandelwal, R. L., & Chibbar, R. N. (2003). Synthesis of novel starches in planta: opportunities and challenges. *Starch-Stärke*, *55*(3-4), 107-120.

Dhondt, S., Wuyts, N., & Inze, D. (2013). Cell to whole-plant phenotyping: the best is yet to come. *Trends in plant science*, *18*(8), 428-439.

Du, H., Henry, P., Ren, X., Cheng, M., Goldman, D. B., Seitz, S. M., & Fox, D. (2011). Interactive 3D modeling of indoor environments with a consumer depth camera. In *Proceedings of the 13th international conference on Ubiquitous computing* (pp. 75-84). ACM.

Efron, B., & Tibshirani, R. J. (1994). *An introduction to the bootstrap*. CRC press.

Ehlert, D., Heisig, M., & Adamek, R. (2010). Suitability of a laser rangefinder to characterize winter wheat. *Precision agriculture*, *11*(6), 650-663.

Ehlert, D., Adamek, R., & Horn, H. J. (2009). Laser rangefinder-based measuring of crop biomass under field conditions. *Precision Agriculture*, *10*(5), 395-408.

Ehlert, D., Horn, H. J., & Adamek, R. (2008). Measuring crop biomass density by laser triangulation. *Computers and electronics in agriculture*, *61*(2), 117-125.

Eitel, J. U., Magney, T. S., Vierling, L. A., Brown, T. T., & Huggins, D. R. (2014). LiDAR based biomass and crop nitrogen estimates for rapid, non-destructive assessment of wheat nitrogen status. *Field Crops Research*, *159*, 21-32.

Eitel, J. U., Vierling, L. A., Long, D. S., & Hunt, E. R. (2011). Early season remote sensing of wheat nitrogen status using a green scanning laser. *Agricultural and Forest Meteorology*, *151*(10), 1338-1345.

Eiumnoh, A., & Shrestha, R. P. (1999). A Study on Estimation of Cassava Area and Production Using Remote Sensing and Geographic Information Systems in the Northeast Region of Thailand. *Japanese Journal of Southeast Asian Studies*, *37*(3), 417-430.

El-Sharkawy, M. A. (2003). Cassava biology and physiology. *Plant molecular biology*, *53*(5), 621-641.

Ellis, R. P., Cochrane, M. P., Dale, M. F. B., Duffus, C. M., Lynn, A., Morrison, I. M., ... & Tiller, S. A. (1998). Starch production and industrial use. *Journal of the Science of Food and Agriculture*, *77*(3), 289-311.

Elsayed, S., Mistele, B., & Schmidhalter, U. (2011). Can changes in leaf water potential be assessed spectrally?. *Functional Plant Biology*, *38*(6), 523-533.

Eric, N., & Jang, J. W. (2017). Kinect depth sensor for computer vision applications in autonomous vehicles. In *2017 Ninth International Conference on Ubiquitous and Future Networks (ICUFN)* (pp. 531-535). IEEE.

Fauquet, C., & Fargette, D. (1990). African cassava mosaic virus: etiology, epidemiology and control. *Plant Dis*, *74*(6), 404-411.

Fiorani, F., & Schurr, U. (2013). Future scenarios for plant phenotyping. *Annual review of plant biology*, *64*, 267-291.

Freeman, K. W., Girma, K., Arnall, D. B., Mullen, R. W., Martin, K. L., Teal, R. K., & Raun, W. R. (2007). By-plant prediction of corn forage biomass and nitrogen uptake at various growth stages using remote sensing and plant height. *Agronomy Journal*, *99*(2), 530-536.

Friedli, M., Kirchgessner, N., Grieder, C., Liebisch, F., Mannale, M., & Walter, A. (2016). Terrestrial 3D laser scanning to track the increase in canopy height of both monocot and dicot crop species under field conditions. *Plant Methods*, *12*(1), 9.

Fukuda, W. M. G., Guevara, C. L., Kawuki, R., & Ferguson, M. E. (2010). *Selected morphological and agronomic descriptors for the characterization of cassava*. IITA.

Furbank, R. T. (2009). Plant phenomics: from gene to form and function. *Functional Plant Biology*, *36*(10), 5-6.

Furbank, R. T., von Caemmerer, S., Sheehy, J., & Edwards, G. (2009). C4 rice: a challenge for plant phenomics. *Functional Plant Biology*, *36*(11), 845-856.

Furbank, R. T., & Tester, M. (2011). Phenomics–technologies to relieve the phenotyping bottleneck. *Trends in plant science*, *16*(12), 635-644.

Galna, B., Barry, G., Jackson, D., Mhiripiri, D., Olivier, P., & Rochester, L. (2014). Accuracy of the Microsoft Kinect sensor for measuring movement in people with Parkinson's disease. *Gait & posture*, *39*(4), 1062-1068.

Geerse, D. J., Coolen, B. H., & Roerdink, M. (2015). Kinematic validation of a multi-Kinect v2 instrumented 10-meter walkway for quantitative gait assessments. *PloS one*, *10*(10), e0139913.

Godfray, H. C. J., Beddington, J. R., Crute, I. R., Haddad, L., Lawrence, D., Muir, J. F., ... & Toulmin, C. (2010). Food security: the challenge of feeding 9 billion people. *science*, *327*(5967), 812-818.

Gokturk, S. B., & Tomasi, C. (2004_a). 3D head tracking based on recognition and interpolation using a time-of-flight depth sensor. In *Proceedings of the 2004 IEEE Computer Society Conference on Computer Vision and Pattern Recognition, 2004. CVPR 2004.* (Vol. 2, pp. II-II). IEEE.

Gokturk, S. B., Yalcin, H., & Bamji, C. (2004_b). A time-of-flight depth sensor-system description, issues and solutions. In *2004 Conference on Computer Vision and Pattern Recognition Workshop* (pp. 35-35). IEEE.

Graham-Rowe, D. (2011). Beyond food versus fuel. *Nature*, *474*(7352), S6.

Gutierrez, S., & Marroquín, J. L. (2004). Robust approach for disparity estimation in stereo vision. *Image and Vision Computing*, *22*(3), 183-195.

Hackenberg, J., Wassenberg, M., Spiecker, H., & Sun, D. (2015). Non destructive method for biomass prediction combining TLS derived tree volume and wood density. *Forests*, *6*(4), 1274-1300.

Han, J., Shao, L., Xu, D., & Shotton, J. (2013). Enhanced computer vision with microsoft kinect sensor: A review. *IEEE transactions on cybernetics*, *43*(5), 1318-1334.

Henry, P., Krainin, M., Herbst, E., Ren, X., & Fox, D. (2014). RGB-D mapping: Using depth cameras for dense 3D modeling of indoor environments. In *Experimental robotics* (pp. 477-491). Springer, Berlin, Heidelberg.

Hoffmeister, D., Waldhoff, G., Korres, W., Curdt, C., & Bareth, G. (2016). Crop height variability detection in a single field by multi-temporal terrestrial laser scanning. *Precision agriculture*, *17*(3), 296-312.

Hoffmeister, D., Bolten, A., Curdt, C., Waldhoff, G., & Bareth, G. (2010). High-resolution Crop Surface Models (CSM) and Crop Volume Models (CVM) on field level by terrestrial laser scanning. In *Sixth International Symposium on Digital Earth: Models, Algorithms, and Virtual Reality* (Vol. 7840, p. 78400E). International Society for Optics and Photonics.

Höfle, B. (2013). Radiometric correction of terrestrial LiDAR point cloud data for individual maize plant detection. *IEEE Geoscience and Remote Sensing Letters*, *11*(1), 94-98.

Holman, F., Riche, A., Michalski, A., Castle, M., Wooster, M., & Hawkesford, M. (2016). High throughput field phenotyping of wheat plant height and growth rate in field plot trials using UAV based remote sensing. *Remote Sensing*, *8*(12), 1031.

Horaud, R., Hansard, M., Evangelidis, G., & Ménier, C. (2016). An overview of depth cameras and range scanners based on time-of-flight technologies. *Machine vision and applications*, *27*(7), 1005-1020.

Hosoi, F., Nakabayashi, K., & Omasa, K. (2011). 3-D modeling of tomato canopies using a high-resolution portable scanning lidar for extracting structural information. *Sensors*, *11*(2), 2166-2174.

Hosoi, F., & Omasa, K. (2009). Estimating vertical plant area density profile and growth parameters of a wheat canopy at different growth stages using three-dimensional portable lidar imaging. *ISPRS Journal of Photogrammetry and Remote Sensing*, *64*(2), 151-158.

Houle, D., Govindaraju, D. R., & Omholt, S. (2010). Phenomics: the next challenge. *Nature reviews genetics*, *11*(12), 855.

Islam, A. T., Scheel, C., Pajarola, R., & Staadt, O. (2017). Robust enhancement of depth images from depth sensors. *Computers & Graphics*, *68*, 53-65.

Jiang, Y., Li, C., & Paterson, A. H. (2016). High throughput phenotyping of cotton plant height using depth images under field conditions. *Computers and Electronics in Agriculture*, *130*, 57-68.

Jones, B., Sodhi, R., Murdock, M., Mehra, R., Benko, H., Wilson, A., ... & Shapira, L. (2014). RoomAlive: magical experiences enabled by scalable, adaptive projector-camera units. In *Proceedings of the 27th annual ACM symposium on User interface software and technology* (pp. 637-644). ACM.

Kanwal, N., Bostanci, E., Currie, K., & Clark, A. F. (2015). A navigation system for the visually impaired: a fusion of vision and depth sensor. *Applied bionics and biomechanics*, *2015*.

Kazmi, W., Foix, S., Alenyà, G., & Andersen, H. J. (2014). Indoor and outdoor depth imaging of leaves with time-of-flight and stereo vision sensors: Analysis and comparison. *ISPRS journal of photogrammetry and remote sensing*, *88*, 128-146.

Keightley, K. E., & Bawden, G. W. (2010). 3D volumetric modeling of grapevine biomass using Tripod LiDAR. *Computers and Electronics in Agriculture*, *74*(2), 305-312.

Klose, R., Penlington, J., & Ruckelshausen, A. (2009). Usability study of 3D time-of-flight cameras for automatic plant phenotyping. *Bornimer Agrartechnische Berichte*, *69*(93-105), 12.

Kowalski, M., Naruniec, J., & Daniluk, M. (2015). Livescan3d: A fast and inexpensive 3d data acquisition system for multiple kinect v2 sensors. In *2015 International Conference on 3D Vision* (pp. 318-325). IEEE.

Kruasilp, J., & Rungsipanich, A. (2010). Evaluation of Cassava plantation area using Rule-based classification of multi-temporal satellite imagery.

Kunz, A., Brogli, L., & Alavi, A. (2016). Interference measurement of kinect for xbox one. In *Proceedings of the 22nd ACM Conference on Virtual Reality Software and Technology* (pp. 345-346). ACM.

Kurakin, A., Zhang, Z., & Liu, Z. (2012). A real time system for dynamic hand gesture recognition with a depth sensor. In *2012 Proceedings of the 20th European signal processing conference (EUSIPCO)* (pp. 1975-1979). IEEE.

Lachat, E., Macher, H., Landes, T., & Grussenmeyer, P. (2015$_a$). Assessment and calibration of a RGB-D camera (Kinect v2 Sensor) towards a potential use for close-range 3D modeling. *Remote Sensing*, *7*(10), 13070-13097.

Lachat, E., Macher, H., Mittet, M. A., Landes, T., & Grussenmeyer, P. (2015$_b$). First experiences with Kinect v2 sensor for close range 3D modelling. *The International Archives of Photogrammetry, Remote Sensing and Spatial Information Sciences*, *40*(5), 93.

LAStools. “Efficient LiDAR Processing Software.” version 141017, academic, obtained from Http://rapidlasso.com/LAStools.

Lattepanda. “A Windows 10 Computer with Integrated Arduino.” Obtained from https://www.lattepanda.com/

Lee, J., Jin, L., Park, D., & Chung, Y. (2016). Automatic recognition of aggressive behavior in pigs using a kinect depth sensor. *Sensors*, *16*(5), 631.

Lerma, J. L., Navarro, S., Cabrelles, M., & Villaverde, V. (2010). Terrestrial laser scanning and close range photogrammetry for 3D archaeological documentation: the Upper Palaeolithic Cave of Parpalló as a case study. *Journal of Archaeological Science*, *37*(3), 499-507.

Li, F., Mistele, B., Hu, Y., Chen, X., & Schmidhalter, U. (2014). Reflectance estimation of canopy nitrogen content in winter wheat using optimised hyperspectral spectral indices and partial least squares regression. *European Journal of Agronomy*, *52*, 198-209.

Li, L. (2014). Time-of-flight camera–an introduction. *Technical white paper*, (SLOA190B).

Li, W., Guo, Q., Jakubowski, M. K., & Kelly, M. (2012). A new method for segmenting individual trees from the lidar point cloud. *Photogrammetric Engineering & Remote Sensing*, *78*(1), 75-84.

Lian, T. S., & Cock, J. H. (1979). Cassava plant forms and their associated morphophysiological characters. *MARDI Res. Bull*, *7*, 55-69.

Litkey, P., Liang, X., Kaartinen, H., Hyyppä, J., Kukko, A., Holopainen, M., ... & Suárez, J. (2008). Single-scan TLS methods for forest parameter retrieval. *Proceedings of SilviLaser*, *2008*, 8th.

Ma, L., Zheng, G., Eitel, J. U., Magney, T. S., & Moskal, L. M. (2016). Determining woody-to-total area ratio using terrestrial laser scanning (TLS). *Agricultural and forest meteorology*, *228*, 217-228.

Mack, R. N., & Pyke, D. A. (1979). Mapping Individual Plants with a Field-Portable Digitizer. *Ecology*, *60*(3), 459-461.

Mann, C. (1997). Reseeding the green revolution. *Science*, *277*(5329), 1038-1043.

Montagnac, J. A., Davis, C. R., & Tanumihardjo, S. A. (2009). Nutritional value of cassava for use as a staple food and recent advances for improvement. *Comprehensive reviews in food science and food safety*, *8*(3), 181-194.

Montes, J. M., Melchinger, A. E., & Reif, J. C. (2007). Novel throughput phenotyping platforms in plant genetic studies. *Trends in plant science*, *12*(10), 433-436.

Naranjo-Hernández, J. E., Jiménez-Alonso, F., Clavijo-Jiménez, M., & Gómez-Casado, Ó. (2017). Reference element guidance of autonomous vehicles using 3D laser scanner. *DYNA-Ingeniería e Industria*, *92*(3).

Nassar, N. M. A., & Ortiz, R. (2007). Cassava improvement: challenges and impacts. *The Journal of Agricultural Science*, *145*(2), 163-171.

Nations, U. (2015). World population prospects: The 2015 revision. *United Nations Econ Soc Aff*, *33*(2), 1-66.

Nelson, R., Krabill, W., & Tonelli, J. (1988). Estimating forest biomass and volume using airborne laser data. *Remote sensing of environment*, *24*(2), 247-267.

Nguyen, T., Slaughter, D., Max, N., Maloof, J., & Sinha, N. (2015). Structured light-based 3D reconstruction system for plants. *Sensors*, *15*(8), 18587-18612.

Nguyen, T. H. L., Ngoan, L. D., Bosch, G., Verstegen, M. W. A., & Hendriks, W. H. (2012). Ileal and total tract apparent crude protein and amino acid digestibility of ensiled and dried cassava leaves and sweet potato vines in growing pigs. *Animal feed science and technology*, *172*(3-4), 171-179.

Noonan, P. J., Howard, J., Hallett, W. A., & Gunn, R. N. (2015). Repurposing the Microsoft Kinect for Windows v2 for external head motion tracking for brain PET. *Physics in Medicine & Biology*, *60*(22), 8753.

Nweke, F., Spencer, D. S., & Lynam, J. K. (2002). *The cassava transformation: Africas bestkept secret*.

Okogbenin, E., Setter, T. L., Ferguson, M., Mutegi, R., Ceballos, H., Olasanmi, B., & Fregene, M. (2013). Phenotypic approaches to drought in cassava. *Frontiers in physiology*, *4*, 93.

Okogbenin, E., Ekanayake, I. J., & Porto, M. C. M. (2003). Genotypic variability in adaptation responses of selected clones of cassava to drought stress in the Sudan savanna zone of Nigeria. *Journal of Agronomy and Crop Science*, *189*(6), 376-389.

Okogbenin, E., & Fregene, M. (2002). Genetic analysis and QTL mapping of early root bulking in an F 1 population of non-inbred parents in cassava (Manihot esculenta Crantz). *Theoretical and Applied Genetics*, *106*(1), 58-66.

Otte, K., Kayser, B., Mansow-Model, S., Verrel, J., Paul, F., Brandt, A. U., & Schmitz-Hübsch, T. (2016). Accuracy and reliability of the kinect version 2 for clinical measurement of motor function. *PloS one*, *11*(11), e0166532.

Ouédraogo, M. M., Degré, A., Debouche, C., & Lisein, J. (2014). The evaluation of unmanned aerial system-based photogrammetry and terrestrial laser scanning to generate DEMs of agricultural watersheds. *Geomorphology*, *214*, 339-355.

Pask, A. J. D., Pietragalla, J., Mullan, D. M., & Reynolds, M. P. (2012). *Physiological breeding II: a field guide to wheat phenotyping*. Cimmyt.

Perez-Gutierrez, C., Martínez-Fernández, J., Sanchez, N., & Álvarez-Mozos, J. (2007). Modeling of soil roughness using terrestrial laser scanner for soil moisture retrieval. In *2007 IEEE International Geoscience and Remote Sensing Symposium* (pp. 1877-1880). IEEE.

Popescu, S. C. (2007). Estimating biomass of individual pine trees using airborne lidar. *Biomass and Bioenergy*, *31*(9), 646-655.

Popescu, S. C., Wynne, R. H., & Nelson, R. F. (2003). Measuring individual tree crown diameter with lidar and assessing its influence on estimating forest volume and biomass. *Canadian journal of remote sensing*, *29*(5), 564-577.

Pound, M. P., French, A. P., Murchie, E. H., & Pridmore, T. P. (2014). Automated recovery of three-dimensional models of plant shoots from multiple color images. *Plant physiology*, *166*(4), 1688-1698.

Prochnik, S., Marri, P. R., Desany, B., Rabinowicz, P. D., Kodira, C., Mohiuddin, M., ... & Rokhsar, D. S. (2012). The cassava genome: current progress, future directions. *Tropical plant biology*, *5*(1), 88-94.

R Core Team (2017). R: A language and environment for statistical computing. R Foundation for Statistical Computing, Vienna, Austria. URL https://www.R-project.org/.

Rocchini, C. M. P. P. C., Cignoni, P., Montani, C., Pingi, P., & Scopigno, R. (2001). A low cost 3D scanner based on structured light. In *Computer Graphics Forum* (Vol. 20, No. 3, pp. 299-308). Oxford, UK and Boston, USA: Blackwell Publishers Ltd.

Rosell-Polo, J. R., Gregorio, E., Gené, J., Llorens, J., Torrent, X., Arnó, J., & Escolà, A. (2017). Kinect v2 sensor-based mobile terrestrial laser scanner for agricultural outdoor applications. *IEEE/ASME Transactions on Mechatronics*, *22*(6), 2420-2427.

Santos, T., & Ueda, J. (2013). Automatic 3D plant reconstruction from photographies, segmentation and classification of leaves and internodes using clustering. In *Embrapa Informática Agropecuária-Resumo em anais de congresso (ALICE)*. In: International conference on functional-structural plant modles, 7., 2013, Saariselkä. Proceedings... Vantaa: Finnish Society of Forest Science, 2013.

Santos, T. T., & De Oliveira, A. A. (2012). Image-based 3D digitizing for plant architecture analysis and phenotyping. In *Embrapa Informática Agropecuária-Artigo em anais de congresso (ALICE)*. In: conference on graphics, patterns and images, 25., 2012, Ouro Preto. Workshop on industry applications. [Sl]: Conference Publishing Series, 2012.

Sayre, R., Beeching, J. R., Cahoon, E. B., Egesi, C., Fauquet, C., Fellman, J., ... & Maziya-Dixon, B. (2011). The BioCassava plus program: biofortification of cassava for sub-Saharan Africa. *Annual review of plant biology*, *62*, 251-272.

Shah, D., Tang, L., Gai, J., & Putta-Venkata, R. (2016). Development of a mobile robotic phenotyping system for growth chamber-based studies of genotype x environment interactions. *IFAC-PapersOnLine*, *49*(16), 248-253.

Sudarman, A., Hayashida, M., Puspitaning, I. R., Jayanegara, A., & Shiwachi, H. (2016). The use of cassava leaf silage as a substitute for concentrate feed in sheep. *Tropical animal health and production*, *48*(7), 1509-1512.

Tanner, H. (2000). *U.S. Patent No. 6,145,509*. Washington, DC: U.S. Patent and Trademark Office.

Tester, M., & Langridge, P. (2010). Breeding technologies to increase crop production in a changing world. *Science*, *327*(5967), 818-822.

Thoren, D., & Schmidhalter, U. (2009). Nitrogen status and biomass determination of oilseed rape by laser-induced chlorophyll fluorescence. *European Journal of Agronomy*, *30*(3), 238-242.

Tilly, N., Hoffmeister, D., Cao, Q., Huang, S., Lenz-Wiedemann, V., Miao, Y., & Bareth, G. (2014). Multitemporal crop surface models: accurate plant height measurement and biomass estimation with terrestrial laser scanning in paddy rice. *Journal of Applied Remote Sensing*, *8*(1), 083671.

Vázquez-Arellano, M., Reiser, D., Paraforos, D. S., Garrido-Izard, M., Burce, M. E. C., & Griepentrog, H. W. (2018). 3-D reconstruction of maize plants using a time-of-flight camera. *Computers and Electronics in Agriculture*, *145*, 235-247.

Wanapat, M. (2002). The role of cassava hay as animal feed. *DOA CIAT*, 504.

Watanabe, T., Hanan, J. S., Room, P. M., Hasegawa, T., Nakagawa, H., & Takahashi, W. (2005). Rice morphogenesis and plant architecture: measurement, specification and the reconstruction of structural development by 3D architectural modelling. *Annals of botany*, *95*(7), 1131-1143.

Watt, P. J., & Donoghue, D. N. M. (2005). Measuring forest structure with terrestrial laser scanning. *International Journal of Remote Sensing*, *26*(7), 1437-1446.

Wholey, D. W., & Cock, J. H. (1974). Onset and rate of root bulking in cassava. *Experimental Agriculture*, *10*(3), 193-198.

Wilson, M. (2017). Exclusive: Microsoft has stopped manufacturing the kinect. *Co. Design*, *25*.

Wolfram, C., Shelef, O., & Gertler, P. (2012). How will energy demand develop in the developing world?. *Journal of Economic Perspectives*, *26*(1), 119-38.

Yang, W., Xu, X., Duan, L., Luo, Q., Chen, S., Zeng, S., & Liu, Q. (2011). High-throughput measurement of rice tillers using a conveyor equipped with x-ray computed tomography. *Review of Scientific Instruments*, *82*(2), 025102.

Yoshida, M., & Nagasawa, R. (2010). Analysis on the cassava cropping system using temporal ALOS images: A case study in Nakhon Ratchasima, Thailand. *Journal of the Japanese Agricultural Systems Society (Japan)*.

Zennaro, S., Munaro, M., Milani, S., Zanuttigh, P., Bernardi, A., Ghidoni, S., & Menegatti, E. (2015). Performance evaluation of the 1st and 2nd generation Kinect for multimedia applications. In *2015 IEEE International Conference on Multimedia and Expo (ICME)* (pp. 1-6). IEEE.

Zhang, L., & Grift, T. E. (2012). A LIDAR-based crop height measurement system for Miscanthus giganteus. *Computers and electronics in agriculture*, *85*, 70-76.

Zhang, K., Chen, S. C., Whitman, D., Shyu, M. L., Yan, J., & Zhang, C. (2003). A progressive morphological filter for removing nonground measurements from airborne LIDAR data. *IEEE transactions on geoscience and remote sensing*, *41*(4), 872-882.

Zhu, J., Wang, L., Yang, R., & Davis, J. (2008). Fusion of time-of-flight depth and stereo for high accuracy depth maps. In *2008 IEEE Conference on Computer Vision and Pattern Recognition* (pp. 1-8). IEEE.